https://doi.org/10.7795/120.20220324

Technical Report

The PTB free-air ionization chambers

L. Büermann

Physikalisch-Technische Bundesanstalt
Bundesallee 100, 38116 Braunschweig, Germany

ABSTRACT: The fundamental quantity in the dosimetry of ionizing radiation is the absorbed dose to matter in units of J/kg with the special name of *gray* (Gy). The Physikalisch-Technische Bundesanstalt (PTB), the national metrology institute of Germany, is responsible for the realization and dissemination of the gray for x- and gamma radiation. The quantity air kerma is the metrological basis for dosimetry in radiation protection applications as well as in medical x-ray diagnostics and therapy. Air kerma for x-radiation is primarily measured using what are known as free-air ionization chambers (FACs). This technical report describes the definition of air kerma, the physical principles behind FACs, the technical design of three different FACs maintained at PTB, and the procedures and data needed to obtain the air kerma from the charge measured by FACs. This report is of general interest not only for researchers at other national metrology institutes who work with FACs but also for anyone who has air kerma calibration done for their secondary air kerma standards with traceability to FACs.

KEYWORDS: Dosimetry concepts and apparatus; X-ray detectors; Models and simulations; X-ray generators and sources; Radiation monitoring.

Contents

1 Introduction

The Physikalisch-Technische Bundesanstalt (PTB) is the national metrology institute of Germany. One of their most important tasks is the realization and dissemination of fundamental quantities and units. Air kerma is a fundamental quantity in the dosimetry of ionizing radiation, forming the basis for dosimetry in radiation protection applications as well as in x-ray diagnostics and therapy. Operational quantities in radiation protection, like ambient- or personal-dose equivalent, are obtained from the air kerma by means of calculated conversion factors. Application-specific dose quantities in x-ray diagnostics, including incident air kerma, air kerma-length or air kerma-area product, are based on air kerma. The basic quantity in kilovoltage x-ray beam dosimetry is absorbed dose to water, which is most frequently derived from the air kerma multiplied by calculated conversion factors.

PTB operates a set of three free-air ionization chambers (FACs) which are suitable for air kerma measurements for x-radiation qualities generated with tube voltages in the range of 7.5 kV to 400 kV. This range covers the calibration of secondary standards used in radiation protection (7.5 kV – 400 kV), x-ray diagnostics (20 kV – 150 kV) and therapy (7.5 kV – 300 kV). PTB calibrates secondary air kerma standards for clients around the world. These include other national metrology institutes who do not maintain their own primary standards and use the PTB-calibrated standards as their national air kerma standards. Further, the International Atomic Energy Agency (IAEA) uses secondary standards calibrated at PTB to calibrate the standards of the worldwide network of Secondary Standard Dosimetry Laboratories (SSDLs). Finally, other accredited SSDLs make use of PTB's calibration service.

This technical report describes in detail the primary standard free-air ionization chambers at PTB. In section 2 the fundamental quantity air kerma and its relation to the quantity exposure is introduced. Section 3 deals with the basic principles of FACs and with the evaluation of the general correction factors needed to determine the air kerma from the measured charge of the chamber. Finally, section 4 contains detailed technical descriptions of PTB's three FACs. Here, the determination by measurement and calculation of all relevant correction factors will be described and the results presented. The uncertainty components of air kerma determination with the FACs are evaluated and the combined uncertainties of the air kerma presented. A summary of all results is given in section 5.

2 Air kerma and exposure

The fundamental quantities of kerma (kinetic energy released per mass) and exposure are defined in ICRU Report 85 [1]. Because the realization of the units of these quantities by primary standard measurement facilities is the subject of this technical report, the definitions will be repeated here, but with the general definitions adapted to the special case of photons in air.

The kerma for photons in air K_{air} is the quotient of $\mathrm{d}E_{\mathrm{tr}}$ by $\mathrm{d}m_{\mathrm{air}}$, where $\mathrm{d}E_{\mathrm{tr}}$ is the mean sum of the initial kinetic energies of all the electrons liberated in a mass of air $\mathrm{d}m_{\mathrm{air}}$ by the photons incident on $\mathrm{d}m_{\mathrm{air}}$, thus

$$K_{\mathrm{air}}=\frac{\mathrm{d}E_{tr}}{\mathrm{d}m_{\mathrm{air}}} \tag{1}$$

The unit of the air kerma is J/kg or gray (Gy). The air kerma rate is the quotient of $\mathrm{d}K_{\mathrm{air}}$ by $\mathrm{d}t$, where $\mathrm{d}K_{\mathrm{air}}$ is the increment of air kerma in the time interval $\mathrm{d}t$, thus

$$\dot{K}_{\mathrm{air}}=\frac{\mathrm{d}K_{\mathrm{air}}}{\mathrm{d}t} \tag{2}$$

The quantity $\mathrm{d}E_{\mathrm{tr}}$ includes the kinetic energy of Auger or Coster-Kronig electrons emitted in the decay of excited atoms or molecules.

For a fluence ϕ of photons of energy E, the air kerma K_{air} is given by

$$K_{\mathrm{air}}=\Phi E\frac{\mu_{\mathrm{tr}}}{\varrho_{\mathrm{air}}} \tag{3}$$

where μ_{tr}/ρ_{air} is the mass energy-transfer coefficient of air for photons. K_{air}/Φ is termed the air kerma coefficient for photons. For a distribution Φ_E of photon fluence with respect to energy, the air kerma is given by

$$K_{air} = \int \Phi_E E \frac{\mu_{tr}}{\varrho_{air}} \mathrm{d}E \tag{4}$$

The air kerma corrected for radiative losses is called the collision air kerma $K_{col,air}$ and is given by

$$K_{col,air} = \Phi E \frac{\mu_{en}}{\rho_{air}} = \Phi E \frac{\mu_{tr}}{\rho_{air}} (1\text{-}\bar{g}) = K_{air} (1\text{-}\bar{g}) \tag{5}$$

where μ_{en}/ρ_{air} is the mass energy-absorption coefficient of air for photons of energy E and g is the fraction of the kinetic energy of the liberated electrons that would be lost in radiative processes in air. The collision air kerma for a distribution ϕ_E of photon fluence with respect to energy is given by

$$K_{col,air} = \int \Phi_E E \frac{\mu_{en}}{\rho_{air}} \mathrm{d}E = \int \Phi_E E \frac{\mu_{tr}}{\rho_{air}} (1\text{-}\bar{g})\, \mathrm{d}E = K_{air} (1\text{-}\bar{g}) \tag{6}$$

where $\bar{g}$ is the mean value of g averaged over the distribution of the kerma with respect to the electron energy.

The exposure X is the quotient of dq by dm_{air}, where dq is the absolute value of the mean total charge of the ions of one sign produced when all the electrons and positrons liberated or created by photons incident on a mass of dry air dm_{air} are completely stopped in dry air, thus

$$X = \frac{\mathrm{d}q}{\mathrm{d}m_{air}} \tag{7}$$

The ionization produced by electrons emitted in atomic/molecular relaxation processes is included in dq, whereas the ionization due to photons emitted by radiative processes (i.e., bremsstrahlung and fluorescence photons) is not. Except for this difference, which is significant at high energies, the exposure as derived above is the ionization analogue of the dry-air kerma, which can be expressed by

$$X \approx \frac{e}{W_{air}} K_{air,col} \tag{8}$$

where e is the elementary charge and W is the mean energy expended in dry air per ion pair formed. The approximation symbol in eq. (8) reflects the fact that the exposure includes the charge of electrons or ions liberated by the incident photons, whereas W pertains only to the charge produced during the deceleration of these electrons.

3. Air kerma measurements with free-air ionization chambers

3.1 Design and principle of operation

Free-air ionization chambers (FAC) were recently reviewed in detail by Burns and Büermann [2]. The section of this review article that describes the principle of operation of FACs will essentially be repeated here to facilitate the reading of this report. A schematic representation of a parallel-plate free-air chamber is shown in Figure 1. The main elements are an entrance diaphragm with aperture radius r_{ap} and a pair of planar electrodes separated by a distance d. An electric field exists between these electrodes that is produced by applying a polarizing potential (high voltage, HV) to one of the electrodes while the other (G-C-G) is maintained at virtual ground potential. An isolated section of the latter electrode (C), of length l in the beam direction, is connected to a sensitive current measuring apparatus and is referred to here as the collecting electrode, while the remainder of the plate (G) is designated the guard electrode. The collecting electrode and the electrical field lines define a region of length l in which charge is collected. This area is referred to as the collecting region and shown as the shaded area in Figure 1.

The chosen aperture diameter is larger than the dimensions of the photon source, so a divergent beam of primary photons enters the chamber and exits through a hole in the rear wall, this hole being larger than the beam diameter at that point. During their passage, the primary photons generate

secondary electrons. If the electrode separation d is sufficiently large, these electrons cannot reach either electrode and thus come to rest in the air of the chamber, as do all liberated electrons.

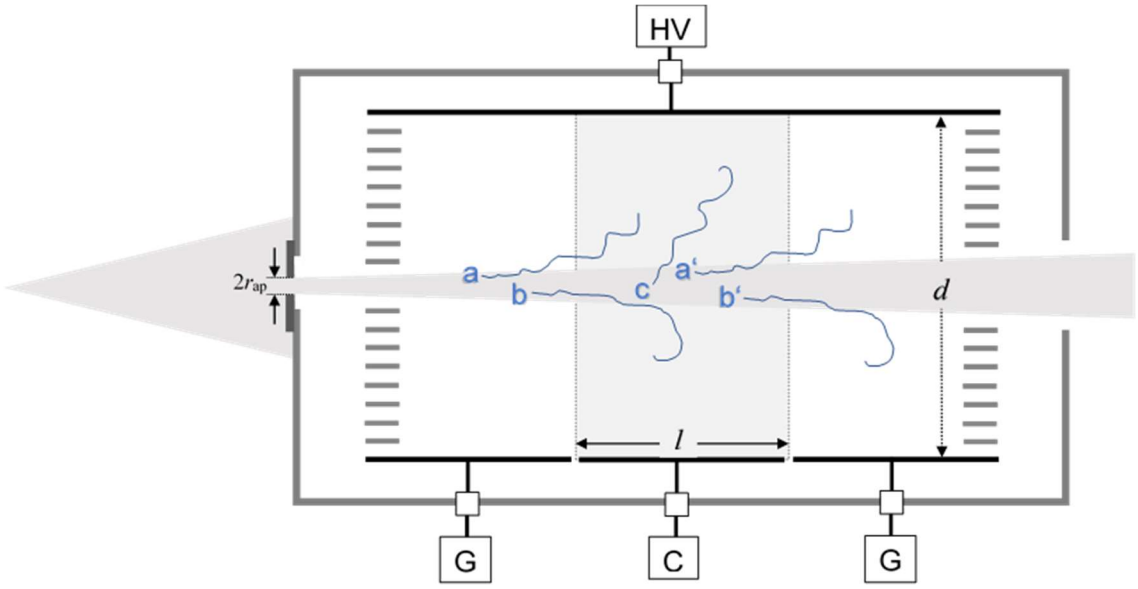

Figure 1. Sketch of a free-air chamber with secondary electron tracks a, b, c, a' and b'.

If the distance between the diaphragm and the collecting region is greater than the maximum secondary-electron range (a similar condition also applies beyond the collecting region), transient charged particle equilibrium (CPE) will exist in the collecting region. This is demonstrated by the secondary electron tracks in the figure. The aim is to measure the sum of the kinetic energies of secondary electrons liberated by primary photon interactions inside the collecting region. Electron *c* is liberated inside the collecting region and loses its total initial kinetic energy inside the collecting region. That is what is wanted. Electrons *a* and *b*, although liberated outside the collecting region, lose parts of their initial kinetic energy along their tracks inside the collecting region. That is an unwanted energy gain. Electrons *a'* and *b'*, liberated inside the collecting region, lose parts of their initial kinetic energy along their tracks outside the collecting region. That represents an unwanted energy loss. CPE means that the energy gain by tracks of type *a* and *b* is exactly compensated by the energy loss by tracks of type *a'* and *b'*. Under these conditions, the charge collected is a measure of the total charge liberated in photon interactions over the length l of the collecting region. In other words, the collected charge is a measure of the exposure for the air mass m_{air}, where

$$m_{air} = \rho_{air} \pi r_{ap}^2 l \tag{9}$$

Here, ρ_{air} is the air density at the time of the measurement.

Note that the product $\pi r_{ap}^2 l$, which appears to represent a volume, does not represent a physical region within the chamber (the volume of intersection of the cone of primary photons and the collecting region is significantly greater than this). The area πr_{ap}^2 is that of the aperture and, when multiplied by the photon energy fluence $\Phi(E)*E$ at the defining (reference) plane of the diaphragm, represents the total energy of photons of energy E entering the chamber. This energy has no dependence on the divergence of the photons within the chamber. The exposure is a measure of the charge liberated by these photons through interactions over the length l. For this procedure to be meaningful, a correction must be applied to the measured charge for photon attenuation between the diaphragm and the collecting region. The quantity determined is then the exposure at the defining plane of the diaphragm. (Strictly speaking, for a photon with angle θ to the beam axis it is the interaction length $l/\cos\theta$ that is relevant.

However, for typical geometries the maximum angle is less than 1° and the error introduced is below 0.01%.)

The air kerma rate in the reference plane is derived from the exposure rate essentially by applying eq. (8):

$$\dot{K}_{\mathrm{air}} = \frac{W_{\mathrm{air}}}{e} \frac{I}{m_{\mathrm{air}}} \frac{1}{1-\bar{g}} \prod_i k_i \tag{10}$$

where the exposure X is replaced by the specific ionization current I / m_{air} and a product of correction factors k_i is introduced to correct for the limitations of the free-air chamber in measuring the exposure rate.

3.2 Correction factors for free-air ionization chambers

3.2.1 General correction factors

The correction factors generally applied to free-air chambers will be explained briefly in this section.

Correction for air density at reference conditions, k_ρ

The air kerma measured with a FAC is usually referred to the density of air at reference air pressure and temperature p_0 and T_0. Let p and T be the air pressure and temperature at the time of measurement. Air is close to an ideal gas for which the density is proportional to p/T; the air density correction, k_ρ, is thus calculated by

$$k_\rho = \frac{p_0 T}{p T_0} \tag{11}$$

where p_0 = 1013.25 hPa and T_0 =293.15 K, the reference air conditions used at PTB.

Correction for the lack of saturation, $k_{\mathrm{s}} = k_{\mathrm{si}} k_{\mathrm{sv}}$, due to initial, k_{si}, and volume, k_{sv}, recombination

It is well known that in FACs the ionization current is reduced through the recombination of ions, and this has to be corrected for. Mechanisms of recombination have been reviewed by Boag [3]. The main pathways for the disappearance of ions are initial and general (or volume) recombination, which must be corrected for by the factors k_{si}.and k_{sv}. The term *initial recombination* is applied to the recombination of positive and negative ions formed within the track of a single ionizing particle. As it is an intratrack process and is independent of the number of tracks formed per second (which is the dose rate), it depends only on the initial ion density in each track and on the field strength normal to the tracks. The term *general* (or *volume*) *recombination* applies to the effect by which some positive and negative ions formed by different ionizing particles meet and recombine as they drift toward the opposite electrodes. Volume recombination increases as the average concentrations of ions of both signs rises, i.e., with increasing dose rate. It is difficult to calculate the recombination loss quantitatively by theoretical models. However, in the near saturation region it is well known that if initial recombination is dominant, one should find a linear relationship between $1/I$ and $1/U$ (eq. 12), but if general recombination is dominant, there should exist a linear relationship between $1/I$ and $1/U^2$ (eq. 13), where I is the ionization current and U is the applied polarizing voltage in both cases.

$$1/I = 1/I_0 + const/U \tag{12}$$

$$1/I = 1/I_0 + const/U^2 \tag{13}$$

In both equations I_0 is the saturation current. The correction factors for initial and volume recombination are determined by measurements of the ionization currents as a function of the applied voltage U at very low and very high dose rates, respectively. At low dose rates, when initial recombination dominates, the validity of eq. (12) is assumed and $1/I$ is plotted against $1/U$. Extrapolation to infinite values of U in the

linear plot yields $1/I_0$. k_{si} is obtained as the ratio $I_0/I(U_0)$, where U_0 is the voltage usually applied to the FAC for measurements. At high dose rates, volume recombination is dominant and eq. (13) is assumed to be valid. $1/I$ is now plotted against $1/U^2$. Applying the same extrapolation procedure as described above yields $k_{\mathrm{sv}} = I_0/I(U_0)$. Multiplying eq. (13) by I_0, and bearing in mind that the chamber current I is approximately equal to I_0 near the saturation region, the following equation is obtained:

$$k_{\mathrm{sv}} = I_0/I = 1 + const/U^2 * I \qquad (14)$$

Correction for humidity in air, k_{h}

The air kerma relates to dry air. However, free-air chambers contain humid air. The correction for the effects of humid air is generally calculated by $k_{\mathrm{h}} = I_{\mathrm{a}} / I_{\mathrm{h}}$, where I_{a} and I_{h} are ionization currents measured in dry and humid air of relative humidity h in both a free-air chamber and a cavity chamber. Values for k_{h} were determined on this basis by Niatel [4], [5] and can be derived from Figure 5.14 of ICRU Report 31 [6], here reproduced in Figure 2. At h = 50%, k_{h} is approximately 0.9980 for the free-air and 0.9970 for the cavity chamber. Because the relative humidity in the laboratory rooms of the PTB is always within the range of 30% to 60%, the humidity correction is taken as 0.9980 for free-air and 0.9970 for cavity chambers, with possible variations taken into account by the uncertainties of approximately 0.05% for free-air and 0.02% for cavity chambers.

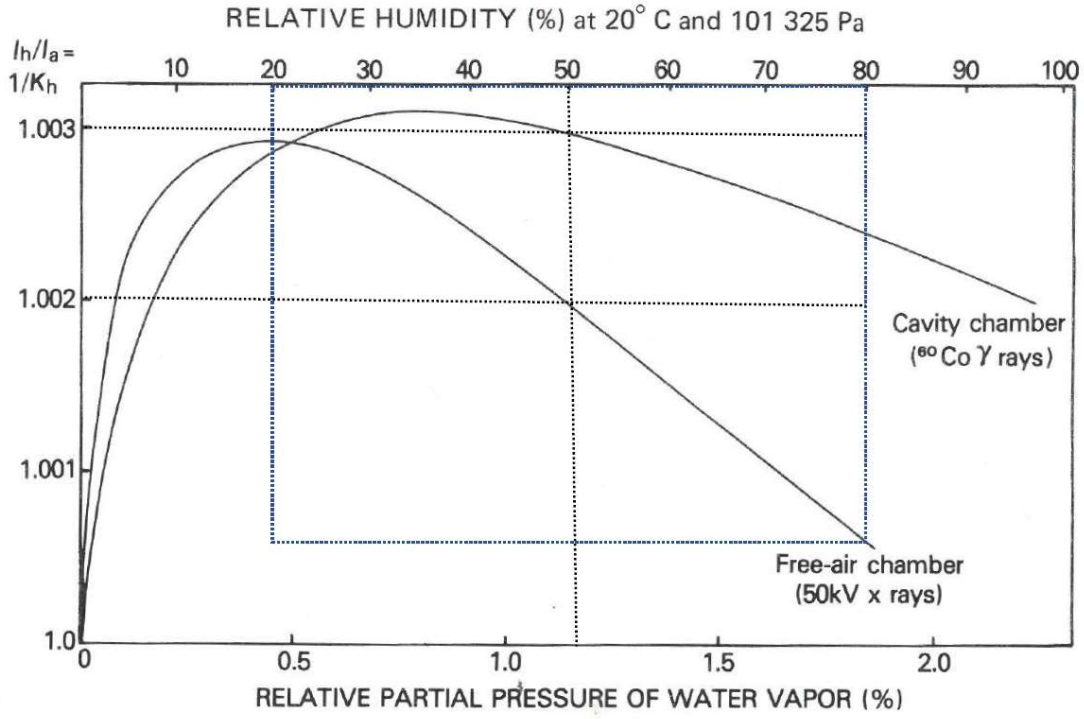

Figure 2. Correction $\boldsymbol{k_{\mathrm{h}}}$ derived from ionization current measurements at different air humidity levels in free-air and cavity chambers (copy of Figure 5.14 from ICRU 31 [6]).

Product of the correction for the initial ion pair and low-energy W_{air} *data,* $k_{\mathrm{ii}}k_{\mathrm{W}}$

The ion pair formed by the initial interaction of the primary photon is included in the measured charge Q of the FAC but has to be corrected for as it must not be included in the calculation of the deposited energy by $\frac{W_{\mathrm{air}}}{e}\frac{Q}{m_{\mathrm{air}}}$ [7], [8]. This is done using the correction factor k_{ii}. The effective W_{air}value at low photon energies deviates from the constant value of 33.97 eV used in eq. (9). These deviations are corrected by k_{W}. As k_{ii} and k_{W} are correlated it make sense to correct for the combined effect expressed by the product $k_{\mathrm{ii}}k_{\mathrm{W}}$.

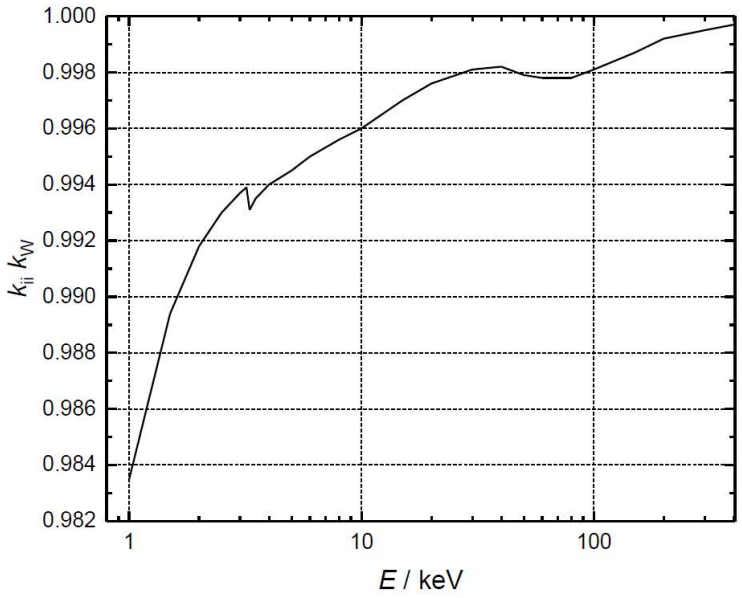

Figure 3. The product $\boldsymbol{k_{ii}k_W}$ as a function of the photon energy E. Data taken from Table 5.7 of ICRU Report 90 [9].

Values of this product calculated by different authors are listed in Table 5.7 of the ICRU Report 90 [9]. For the PTB free-air chambers, the values calculated with the PENELOPE Monte Carlo model described in ICRU Report 90 [9] were adopted and are shown in Figure 3.

Correction for electrical field distortion, k_{d}

Figure 1 clearly shows that the collecting volume strongly depends on the shape of the electrical field lines. The PTB FACs are designed such as to minimize electrical field distortions at the borderlines of the collecting electrodes. This is mainly achieved by the guard electrodes and the guard strips which connect the polarizing electrodes via the resistors of a voltage divider. If necessary, the field homogeneity can be calculated by finite element electrical field simulation programs. Corrections k_{d} for the PTB FACs were determined by other means (see section 4).

Correction for the polarity effect, k_{pol}

First, the ionization currents at positive and negative polarity, I^+ and I^-, are measured. For subsequent measurements with positive chamber voltage, the polarity correction factor is calculated as

$$k_{pol}= \frac{I^+ + I^-}{2I^+} \tag{15}$$

Correction for chamber wall transmission, k_{p}

The PTB FACs are designed such that the front and side walls are covered with lead thick enough to absorb photons which hit the chamber housing outside the aperture region. To confirm the effectiveness of the shielding current, measurements with and without x-ray beam are done using a special diaphragm having a permanently closed aperture. For the PTB FACs it was found that in the useful range of radiation qualities k_{p} = 1.0000(5).

3.2.2 Correction factors calculated with Monte Carlo Methods

The correction factors for scattered radiation k_{sc}, electron loss k_{e}, diaphragm effects k_{dia}, and distortion of the charged particle equilibrium (cpe) k_{cpe}, are usually calculated by Monte Carlo methods. These will be explained by looking at the different secondary electron tracks shown in Figure 4. The figure

illustrates some physical effects in a free-air chamber which must be taken into account when applying corrections of the measured charge to obtain the air kerma. These and some other correction factors specific to the different chamber designs (see section 4) were calculated using Monte Carlo methods. All PTB chambers are designed to accomplish charged particle equilibrium in the collecting region (CR) up to their maximum energy range of use, so $k_{\mathrm{cpe}} = 1$.

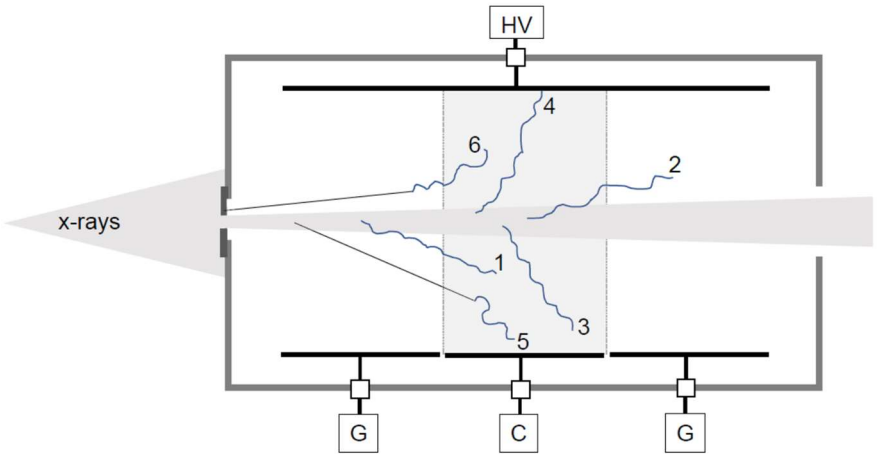

Figure 4. Sketch of a free-air chamber with different electron tracks generated by photon interactions in the air of the chamber. Along their tracks, the electrons lose kinetic energy due to ionization events and produce ion pairs. On average, each ion pair formed in air needs about 34 eV (=J/C). Charge is collected in the shaded collecting region (CR). Depending on the type of electron track involved, the measured charge must be corrected for different effects:

Track 1: An electron produced by a photon interaction outside the CR which deposits parts of its kinetic energy in the CR.

Track 2: An electron produced by a photon interaction inside the CR which deposits parts of its kinetic energy outside the CR. A disbalance of energy depositions in the CR due to type 1 and type 2 tracks gives rise to a disturbed charged particle equilibrium (cpe) and must be corrected by the factor k_{cpe}.

Track 3: An electron produced by a photon interaction inside the CR which deposits its entire kinetic energy in the CR. This is exactly what is wanted so no correction is necessary.

Track 4: An electron is absorbed by the electrode before it can finalize its track in the CR. This represents a loss of deposited energy and is corrected by the factor k_{e}.

Track 5: A scattered photon interacts in the CR and produces an electron which deposits energy in the CR. This contribution is not part of the air kerma and thus the measured charge must be corrected by the factor k_{sc}.

Track 6: A photon transmits through the diaphragm and interacts to produce an electron which deposits energy in the CR. This is an unwanted gain in measured charge and must be corrected for by the factor k_{dia}. This correction is also applied if there are similar contributions from scattered or fluorescence photons escaping from the edge of the aperture.

3.3 Correction factors calculated with the Monte Carlo code system EGS4

Some of the correction factors were calculated by use of the Monte Carlo program EGS4 [10]. This section describes the general methods and the transport data used for this purpose. Details about the EGS4-based chamber-specific user codes are described in section 4.

3.3.1 Principle

Figure 2 shows a sketch of the irradiation geometry typical for free-air chambers. The reference point for the air kerma to be determined with the free-air chamber is defined to be in the centre of a reference plane in the aperture. In the Monte Carlo simulation, a monoenergetic photon source is assumed. Let the beam diameter of the photon radiation be slightly larger than the outer diameter of the aperture body. During the simulation, all primary (not scattered) photons that pass the reference plane from the source through the aperture and into the chamber are counted. Possible scattering of photons in the air between the source and the entrance aperture is not considered, as its influence on the quantity to be calculated is negligible. The air kerma per photon in the reference plane is given by $E\,\mu_{\mathrm{tr}}(E)/\varrho_{\mathrm{air}}$ (see eq. 3), where the energy transfer coefficients of air $\mu_{\mathrm{tr}}(E)/\varrho_{\mathrm{air}}$ were previously determined with a separate EGS4 user code based on the same underlying photon interaction coefficients that were applied for all other user codes for special chamber designs. Using the Monte Carlo simulation of particle transport through the chamber, the mean total energy deposited in the ion collection volume $E_{dep}(E)/\Phi(E)$ of the chamber per primary photon is calculated. In the case of an ideal free-air chamber, this would be equal to $K_{air}/\phi(E) = E\,\mu_{\mathrm{tr}}(E)/\varrho_{\mathrm{air}}$. However, a real free-air chamber suffers from various physical effects (Figure 4) which must be taken into account in order to make corrections to the deposited energy. A calculated theoretical response of a free-air chamber with respect to the air kerma at the reference point can thus be defined as

$$R(E) = E_{dep}(E)/K_{air}(E) \tag{16}$$

The reciprocal of $R(E)$ is the sought correction factor:

$$k(E) = K_{air}(E)/E_{dep}(E) \tag{17}$$

which can alternatively be written as the product of various contributions:

$$k(E) = \prod_i k_i(E) = \prod_i K_{air}(E)/E_{dep,i}(E) \tag{18}$$

where $E_{dep,i}$ is the deposited energy resulting from a simulation where all perturbation effects are turned off except for those of type i. Perturbations in this context are all effects which cause the response of the simulated free-air chamber defined by eq. (16) to deviate from one. A selection of possible disturbances to be simulated can be seen in Figure 4.

3.3.2 The EGS4 Monte Carlo code

EGS4 (Electron Gamma Shower, [10]) is a program package for the Monte Carlo simulation of the coupled transport of photons, electrons and positrons in freely definable geometries and materials for particle energies from a few TeV down to 1 keV for photons and 10 keV for electrons and positrons. The program package consists of a system of subroutines to which users adds their own geometry and output routines as well as their main program, which specifies, among other things, the parameters that control the simulation. The entire package is then bound together to form the user code.

The most important parameters to be defined in the main program are the cutoffs AE, AP, ECUT, and PCUT, and the parameter ESTEPE. AE and AP are lower cutoff energies that are set in PEGS4, the preprocessor of EGS4, which prepares the interaction coefficients of the involved materials above these cutoff energies and stores them in a data file even before the actual simulation calculation starts. During

runtime, the EGS4 user program then accesses this data file as needed. At the same time, during the transport of charged particles, AE and AP serve as lower energy loss thresholds for the generation of secondary particles (electrons and bremsstrahlung photons, respectively), which are then treated separately. Below these energy thresholds, the transport is simulated by the approximation of a continuous energy loss based on the theory of multiple scattering, where the energy loss during an electron step now results from the restricted collision stopping power (Δ=AE) or restricted radiation stopping power (Δ=AP). ESTEPE limits the maximum energy loss during an electron step in this approximation and is given as a constant fraction of the particle's remaining kinetic energy. If the energy of the electrons or positrons falls below ECUT or the energy of the photons falls below PCUT, the simulation is terminated, and the remaining kinetic energy is deposited locally.

The results of electron transport simulations can strongly depend on the step size of the electrons, which are determined by the parameters AE and ESTEPE. The user must therefore set these parameters with appropriate caution. To alleviate this problem, an electron transport algorithm called PRESTA [11] has been added to the EGS4 program package. PRESTA quite significantly reduces the step-size dependence of results in many cases and helps to save computation time because it allows simulation with larger step sizes and no loss of quality. But the use of PRESTA does not completely free the user from step-size dependence, as further research has shown [12]. Therefore, it was recommended to use PRESTA together with the condition ESTEPE=0.01 for high accuracy requirements. In the meantime, the algorithm PRESTA II [13] has been developed, which, according to the authors, captured and solved the step-size dependence. Unfortunately, this algorithm was not yet available at the time of the calculations presented in this report. The above recommendation was therefore followed and the PRESTA package together with the condition ESTEPE=0.01 was used for all calculations in which electron transport plays a role. The cut-off parameters AE, AP, ECUT and PCUT were specified depending on the material and the problem. They are given in the following sections if they are relevant to the results of the calculations.

3.3.3 The EGS4 user code ‘MUEEN’

To be able to calculate correction factors for free-air chambers according to the principle presented in 3.3.1, it is necessary to calculate the coefficients μ/ρ, μ_{tr}/ρ and μ_{en}/ρ for air with the same cross sections and physical models which are used in the user programs for the simulation of radiation transport through the various free-air chambers. For this purpose, the EGS4 user program 'MUEEN' was developed to calculate these coefficients. This required the following steps. First, a cross-sectional data set 'AIR.DAT' for air (see Table 1 for composition) was generated using the PEGS4 preprocessor. The total and partial cross sections for photons, which are in 'AIR.DAT', were read out using the user program 'EXAMIN' included in the EGS4 package. Then the transport of monoenergetic photons in an infinitely extended air-filled space was simulated with 'MUEEN' but only up to the first interaction. The path length to the site of the interaction, the type of interaction, and the fractions of the primary photon's energy that are transferred to scattered photons and electrons are registered. The resulting secondary electrons and scattered photons are not followed up thereafter. Bremsstrahlung losses smaller than 0.2% in the considered energy range up to 450 keV were accounted for by a correction factor.

Table 1. Composition of air used in the input data set for PEGS4.

Atom	Fraction by weight
N (Z=7)	0.7554
O (Z=8)	0.2318
Ar (Z=18)	0.1280

From the data obtained, the desired coefficients μ/ρ, μ_{tr}/ρ and μ_{en}/ρ for air, separated by the type of interaction (Rayleigh scattering, photoelectric effect, Compton effect), could be easily calculated.

The user code 'MUEEN' contains the following extensions that were not part of the standard EGS4 package at the time it was used for the purpose of this report:

- Cross-section data for air were generated using PEGS4NB [14], which is based on the RSICC DLC-136/PHOTX (1989) cross-section data set.
- Photoelectric effect with simulation of fluorescence radiation in air (LX – extension [15], K-fluorescence for air based on the principle of Del Guerra et.al. [16]).
- Coherent and incoherent scattering with consideration of the effects due to the binding energy of electrons (LSCAT – extension [17]).
- The 'PHOTX' cross-section data set was chosen in order to be consistent with the data published by Seltzer [18] for the coefficients μ/ρ, μ_{tr}/ρ and μ_{en}/ρ for air, so the values obtained from 'MUEEN' are consistent with this data set. The above extensions were also used in the EGS4 user programs described below for the simulation of radiative transfer through PTB's free-air chambers.

4. Free-air ionization chambers operated at PTB

4.1 Parallel-plate chamber PK100

The parallel-plate free-air ionization chamber type "PK100" ("**P**arallelplatten**k**ammer", suitable for measurements up to **100** kV), is used for radiation qualities generated with tube voltages in the 7.5 kV to 100 kV range. The chamber was conceived, designed and manufactured at PTB and taken into operation as early as 1954. Since then, it has been used as the primary standard for the determination of the quantity exposure/air kerma.

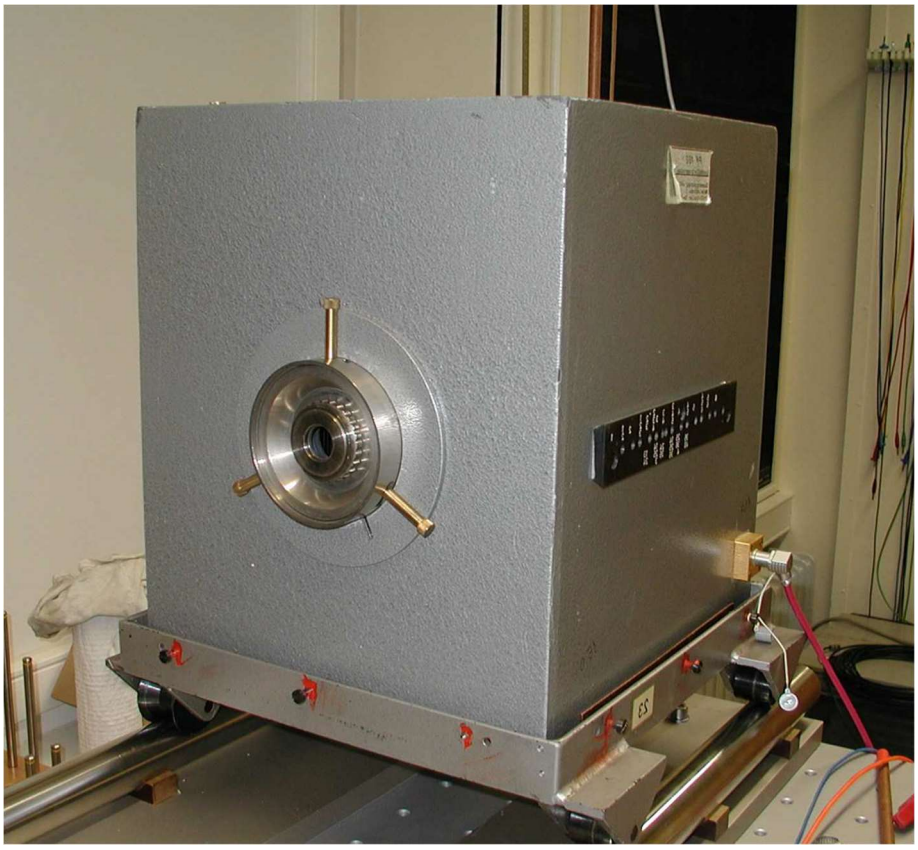

Figure 5. Photo of the free-air chamber type PK100.

4.1.1 Design and dimensions

A schematic overall view of the chamber is shown in Figure 6. The PK100 consists of two rectangular, plane-parallel electrodes E_{HV} and E_G. These are surrounded by the housing H.

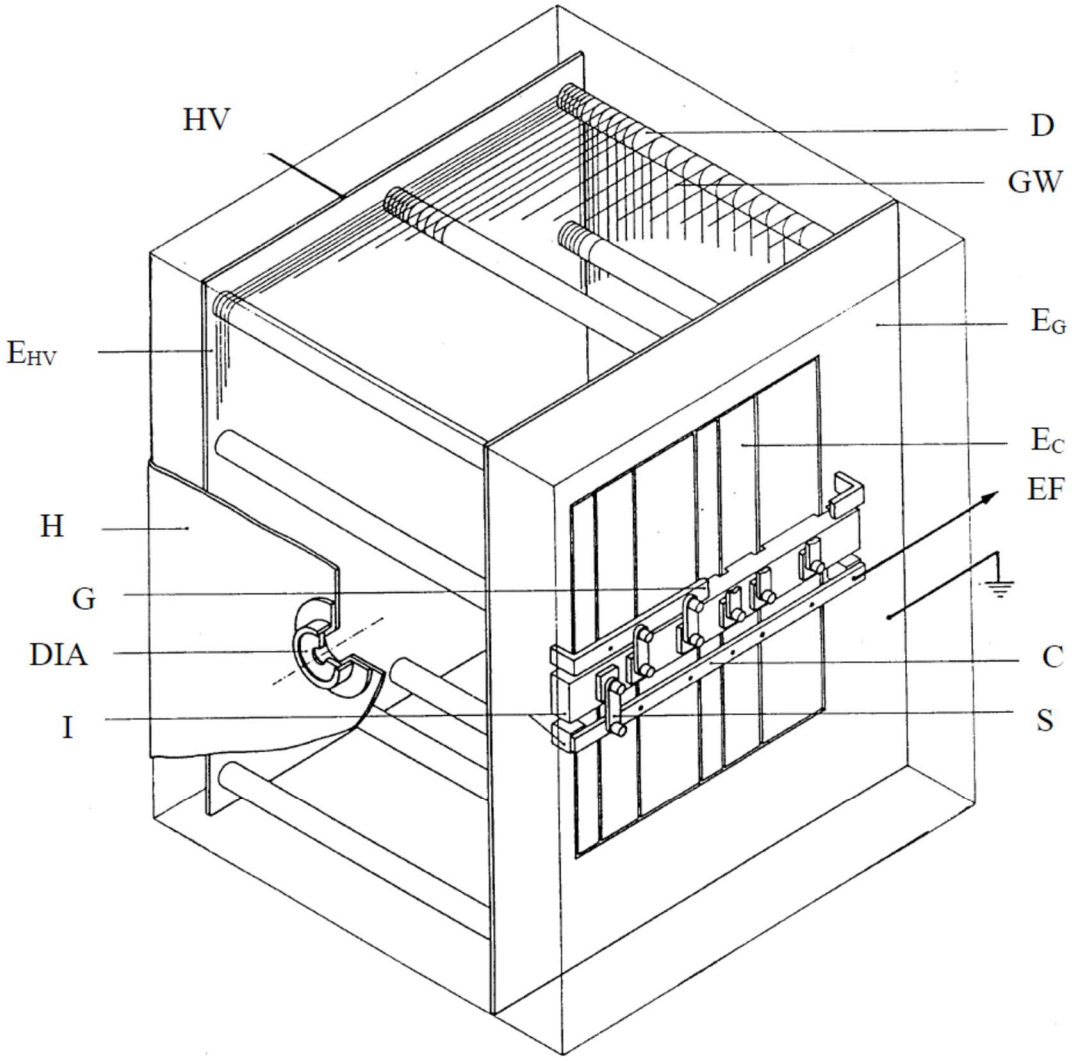

I	Insulator (Trolitul) board
DIA	Diaphragm
G	Grounding board
H	Housing
E_{HV}	High voltage electrode
HV	High voltage connector
D	Distance rods
GW	Guard wires
E_G	Guard electrode
E_C	Collecting electrode
C	Circuit board
S	Switch

Figure 6. Schematic overall view of the PK100

The x-ray beam enters the chamber through the aperture of the diaphragm DIA such that the central axis of the passing x-ray beam is parallel to the electrodes E_{HV} and E_G and equidistant between the pair of electrodes. The x-ray beam leaves the chamber through a circular hole at the rear end of the chamber, which is sealed by a thin 0.03 mm polyethylene (PE) foil. This minimizes backscattering at the rear end of the chamber. The electrodes are made of aluminium covered on the inside with a 0.5 mm thick graphite layer. The dimensions of E_G are 33.0 cm x 38.5 cm and E_{HV} measures 30.8 cm x 36.3 cm. The distance between the electrodes is 23.4 cm. The electrode E_G contains six strips of collecting electrodes E_C separated by 1 mm air gaps and having a height of 24 cm and widths of 2 cm, 3 cm, 5 cm, 2 cm, 3 cm and 5 cm, respectively, in the direction of x-ray beam passage. The remaining part of the electrode E_G serves as a guard electrode. The collecting electrodes are fixed on the insulator board I. They can be connected via switches S either with the grounding board G or circuit board C (the latter leads to the electrometer input). This allows each of the six collecting electrodes to be used separately or to be arbitrarily connected with each other and combined into a longer collecting electrode. In this way it is possible to vary the collecting volume of the chamber as well as the sensitivity.

The applied polarizing high voltage between the electrodes is 6000 V. The guard electrodes are grounded whereas the collecting electrodes may have a little (e.g., 1 mV) potential difference caused by the input amplifier of the electrometer.

The electrical field distortion is minimized by the guard electrode E_G, which is 6.5 cm in width, and the guard wires GW. The guard wires consist of two layers of 77 graphitized nylon threads, 0.25 mm in diameter, which are rolled up 3 mm from each other on plexiglass distance rods D (see Figure 8) in such a way that they connect the electrodes E_{HV} and E_G. The distance rods cause the two layers to be separated by 19 mm, which is given by the diameter of the plexiglass rods. The threads are connected via the resistors (2 MΩ each) of a voltage divider.

The housing H of the chamber is a 2 mm thick aluminium box. The side facing the x-ray source is covered with an 8 mm layer of lead and the remaining sides with 2 mm lead layers. The lead housing attenuates scattered radiation entering the chamber from parts other than the aperture such that their dose contribution in the chamber can be reduced to about 0.1% of the dose caused by the primary beam passing through the aperture.

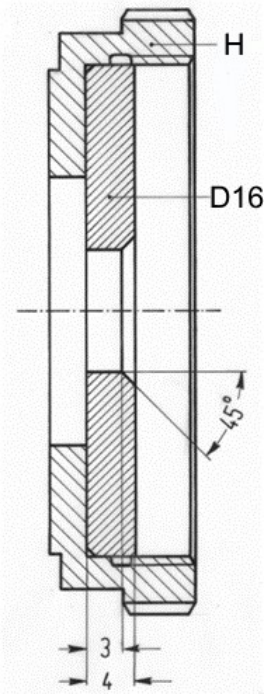

Figure 7. Diaphragm of the PK100.

The diaphragm (see Figure 7 on the left) is made of a tungsten-copper alloy (85% W, 15% Cu) of density 16 g cm $^{-3}$ called D16 (Densimet®). The outer diameter is 41 mm and the thickness is 4 mm. The first 3 mm of the aperture is cylindrical and the last 1 mm is conical with an opening angle of 45° as shown in the figure. The diaphragm holder H is constructed in such a way that the whole assembly can easily be exchanged with another one having a different aperture diameter. Six different apertures are available with nominal circular diameters of 6, 8, 10, 12, 15 and 20 mm.

The measuring volume of the chamber is given by the cylinder which has the diameter of the aperture and the effective width w_{eff} of the collecting electrode. The latter is given by the width of the collector plus half the widths of the air gaps on both sides (2 x 0.5 mm). The reference point of the chamber where the air kerma rate is measured is located on the axis of the aperture at the point where the cylindrical shape transits to the conical one. The distance between the reference point of the chamber and the centre of the collecting electrode is needed for the calculation of the air attenuation correction factor k_{att}. The actual geometrical data of the chamber are given in Tables 2 – 4.

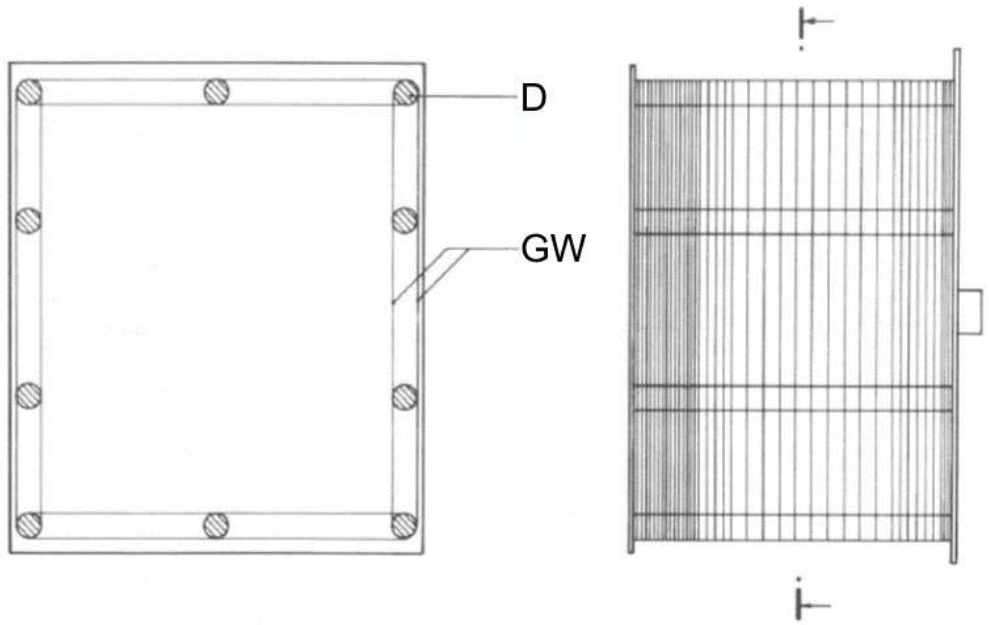

Figure 8. Illustration of the guard wire (GW) assembly of the PK100. The diameter of the plexiglass distance rods (D) is 19 mm.

Table 2. Main dimensions of the parallel-plate free-air ionization chamber PK100.

Item	Dimension
Distance of the polarizing electrodes	23.4 cm
Ground electrode (E_G & E_C), width x height	33.0 cm x 38.5 cm
High voltage electrode (E_{HV}), width x height	30.8 cm x 36.3 cm
Length of the collecting electrode	24.0 cm
Width of the collecting electrodes	See Table 3
Diameter of the apertures	See Table 3
Outer diameter of the diaphragm	41 mm
Thickness of the diaphragm	4.0 mm
Thickness of the graphitized nylon threads (guard wires)	0.25 mm (diameter)
Distance between two nylon threads	3 mm
Thickness of the lead shield at the front of the housing	8 mm
Thickness of the lead shield around the housing (except front wall)	2 mm

Table 3. Measuring volumes of the parallel-plate free-air ionization chamber PK100.

Collecting electrodes		Apertures					
No.	w_{eff} (cm)	0.6 c	0.8 c	1.0 c	1.2 c	1.5 c	2.0 c
		Diameter (cm)					
		0.6005	0.8006	1.0008	1.2013	1.5010	2.0008
		Measuring volumes (cm^3)					
1	2.0021	0.5670	1.0079	1.5748	2.2692	3.5428	6.2947
2	2.9971	0.8487	1.5088	2.3574	3.3969	5.3034	9.4229
3	4.9970	1.4150	2.5156	3.9304	5.6635	8.8421	15.7104
4	2.0011	0.5667	1.0074	1.5740	2.2680	3.5409	6.2914
5	3.0015	0.8500	1.5111	2.3609	3.4014	5.3112	9.4368
6	5.0000	1.4159	2.5171	3.9328	5.6670	8.8474	15.7199
1 - 6	19.9987	5.6632	10.0680	15.7302	22.6665	35.3877	62.8760

Table 4. Air path *A* between the reference point in the aperture and the centre of the collecting electrode of the PK100.

Collecting electrode no.	*A* (cm)
1	9.72
2	12.22
3	16.22
4	19.72
5	22.22
6	26.22
1 - 6	18.72

4.1.2 Chamber model for Monte Carlo simulations

The transport of x-rays through the PK100 was simulated with the Monte Carlo code system EGS4 [10] described in section 3.3. The EGS4-based user code designated "PK100M" was developed for this purpose. The geometrical model used for the simulation is shown in Figure 9. PK100M allows the calculation of the correction factors k_{sc} , k_{e}, k_{dia}, and k_{cpe}, described in section 3, as well as the correction for the attenuation of photons by the guard strips, k_{ap}. Details of the calculation method and results will be given in the following section.

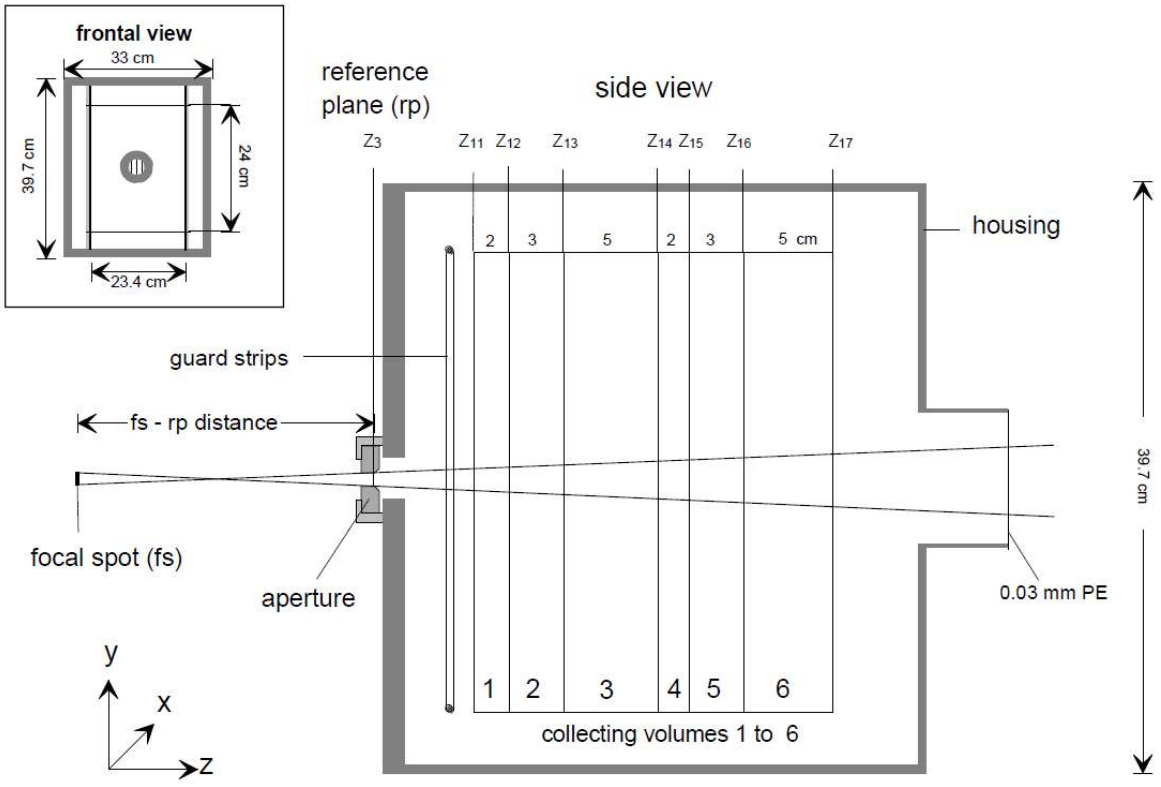

Figure 9. Sketch of the geometry of the PK100 as used in the EGS4-based user code "PK100M".

4.1.3 Correction factors for the PK100

Correction for lack of saturation, k_s

Saturation effects were measured according to the methods described in 3.2. The correction for initial recombination was found to be k_{si}=1.0005(5). The volume recombination was determined for each of the 6 different collecting electrodes and was estimated as

$$k_{SV} = 1 + \frac{R_V(E_{c,n})}{U^2} I_{PK100} \tag{19}$$

where R_V is a constant in units of V^2/A, given for each single collecting electrode $E_{c,n}$, n = 1, 2, …,6, as listed in Table 5, U is the polarizing voltage and I_{PK100} is the chamber current.

The validity of k_{SV} according to eq. (19) and the data given in Table 5 were confirmed experimentally by the following method. The PK100 was positioned at PTB's x-ray calibration facility at a fixed distance from the x-ray tube. For a selected x-radiation quality, the saturation-corrected ionization current of the PK100 was measured at different x-ray tube currents in the 1 mA to 30 mA range.

This caused the ionization current of the PK100 to vary by a factor of 30 and the k_{SV} to vary by up to 3%. The saturation-corrected ionization current of the PK100 was then normalized to the ionization current of the transmission monitor chamber which is always used at the calibration facility and which can be assumed to be characterized by a negligible saturation loss in this ionization current range. The suitability of eq. (19) to determine k_{SV} was confirmed by the fact that the normalization factor remains constant within the uncertainty of the measurements (approximately 0.1%) for all tube currents between 1 mA and 30 mA.

Table 5. The constant $\boldsymbol{R_V}$ for each of the collecting electrodes of the PK100 (U = 6000 V).

Collecting electrode no.	R_V / V^2/A
1	$1.030 * 10^{15}$
2	$4.151 * 10^{14}$
3	$1.367 * 10^{14}$
4	$3.540 * 10^{14}$
5	$2.381 * 10^{14}$
6	$3.023 * 10^{14}$

Correction for electrical field distortion, k_d

Collecting electrode no. 4 (Figure 6) is positioned in the centre of a larger plane parallel capacitor consisting of the guard electrode and high-voltage electrode. The electrical field between this collector plate and the high-voltage electrode can be considered homogeneous because the electrical field lines are almost parallel in the centre of a plane parallel capacitor. The correction for electrical field distortion, k_d, is thus assumed to be 1 for this electrode. The corresponding corrections for the other collecting electrodes were obtained by measurement of their ionization currents, corrected for air density, air attenuation and diaphragm effects, and normalized to their effective widths (in units of A/m) relative to the corresponding values of collecting electrode no. 4. These measurements were done at different radiation qualities generated with tube voltages of not less than 50 kV and at moderate tube currents to keep the air attenuation and saturation effects low. Mean values of the different measurements were taken as the results, which are listed in Table 6.

Table 6. Correction k_{d} for the different collecting electrodes of the PK100.

Collecting electrode no.	w_{eff} (cm)	k_{d}
1	2.0021	0.9910
2	2.9971	0.9938
3	4.9970	0.9969
4	2.0011	1.0000
5	3.0015	0.9905
6	5.0000	0.9934
1 - 6	19.9987	0.9964

Correction for air attenuation between reference and measuring point, k_{att}

The air attenuation correction k_{att} along the air path A is given by

$$k_{att}=e^{\mu_{air}(E)A} \tag{20}$$

where $\mu_{air}(E)$ is the mass attenuation coefficient of air multiplied with the density of air for reference conditions, for a photon of energy E and A is the distance between the reference point and the centre of the collecting region on the axis of the photon beam. Two examples are shown in Figure 10. Usually, x-ray beams emitted from an x-ray tube are used.

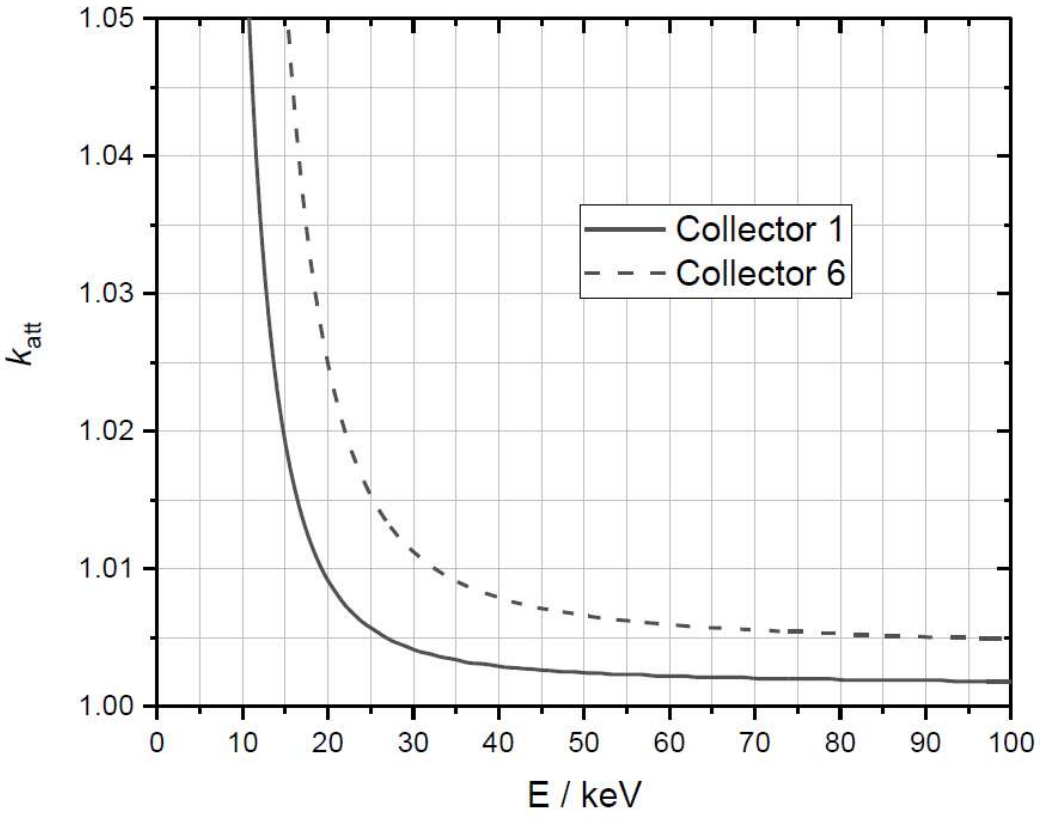

Figure 10. Air attenuation correction k_{att} calculated for the PK100 according to eq. (20) along the path lengths A = 9.72 cm and A = 26.22 cm of collecting electrodes 1 and 6.

At PTB, the photon fluence spectra Φ_E of the radiation qualities in use are measured by means of a high-purity Germanium detector [19]. In this case, k_{att} is calculated by

$$k_{att}=e^{\overline{\mu_{air}}A/k_\rho} \tag{21}$$

where k_ρ is the air density correction factor according to eq. (11) and $\overline{\mu_{air}}$ the fluence-weighted mean value of μ_{air} given by

$$\overline{\mu_{air}} = \frac{\int_0^{E_{max}} \mu_{air}(E)\Phi_E dE}{\int_0^{E_{max}} \Phi_E dE} \tag{22}$$

For radiation qualities generated with tube voltages below 30 kV, the uncertainties in the measured x-ray spectra are larger and $\overline{\mu_{air}}$ was measured by the displacement method as described by Burns and Büermann [2] in section 4.1.1. Note that at PTB, $\overline{\mu_{air}}$ values relate to the reference air density at 20°C and 1013.25 hPa. It is a useful exercise to compare values obtained by calculation according to eq. (22) with those obtained by the displacement method. These should agree within their estimated uncertainties.

Correction for attenuation of photons due to guard strips, k_{ap}

Figure 11 illustrates how photons which pass through the diaphragm are attenuated by the guard strips on their way into the chamber described in 3.3.1. The corrections k_{ap} were calculated by Monte Carlo simulations with the EGS4 code system [10]. They were furthermore measured by means of a dummy construction of the guard strips which can be positioned in front of the aperture. A measurement of the chamber current with and without the dummy in position yields a measured value of k_{ap}. It is important to position the dummy such that the dummy strips are oriented perpendicularly to the real strips in the chamber in order to ensure that the dummy strips are not in line with the real strips. The calculated values were obtained by comparing the air kerma in plane Z_3 to that in plane Z_{11}, as shown in Figure 11. The real strips are graphitized nylon threads 0.25 mm in diameter. For the simulations, pure nylon of a different density was used because the real thickness of the graphite layer is not known. To obtain the density for most closely mimicking the attenuation behaviour of the real strips, simulated values were compared with measured ones at selected radiation qualities until a satisfying agreement was achieved. The advantage of using calculated values is that these are then available as a function of monoenergetic photons, whereas measurements can only be performed for given x-ray spectra. From the values given as a function of monoenergetic photons, mean values can be calculated from measured x-ray spectra. As PTB offers hundreds of different x-ray spectra for calibrations it would be too time consuming to measure k_{ap} for each of them.

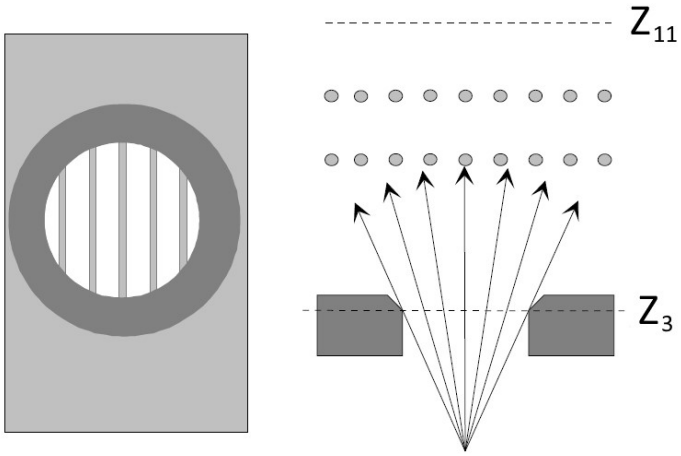

Figure 11. Sketch illustrating the attenuation of photons by the guard strips.

From Figure 11 it is obvious that k_{ap} depends on both the diameter of the aperture and the distance of the focal spot from the reference plane Z_3. The results of calculated values for the different aperture

diameters and distances of 30 cm and 100 cm are shown in Figure 12. For energies higher than 20 keV, k_{ap} decreases to values of about 1.001 and is thus less significant.

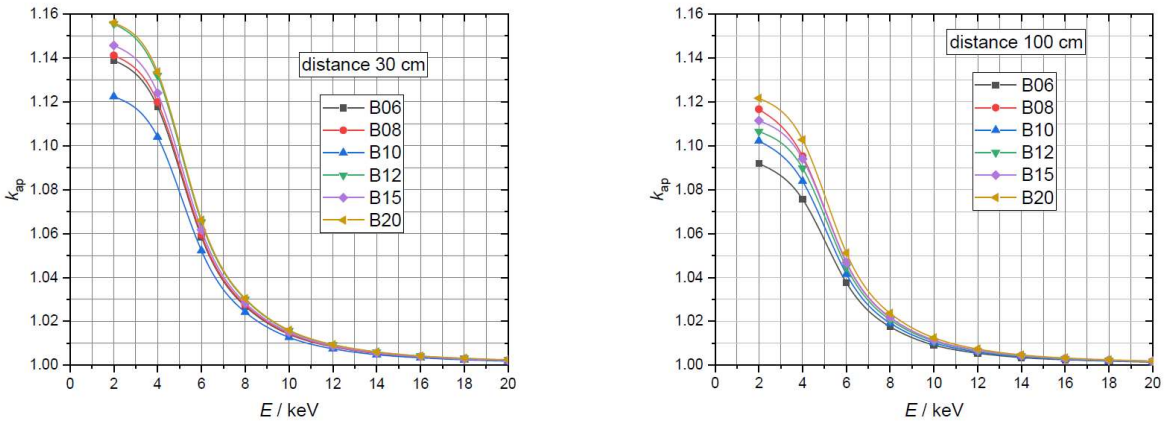

Figure 12. Correction for the attenuation of photons by the guard strips k_{ap} as a function of the photon energy E for apertures B06 (6 mm) to B20 (20 mm). The corrections are significantly larger at a focal spot to aperture reference plane distance of 30 cm (left diagram) than for 100 cm (right diagram).

Correction for diaphragm effects, k_{dia}

The model of the diaphragm used in the PK100M Monte Carlo simulation is shown in Figure 7. Transmission through the 4 mm thick body of the diaphragm made of Densimet® D16 can be neglected for the relevant photons with energies up to 100 keV. However, there are two physical effects which need to be corrected for by k_{dia}, namely the transmission and scattering of photons at the edges of the aperture where the cylindrical shape transits to the conical shape. Further, photoelectric absorption of photons will leave excited W and Cu atoms that subsequently emit fluorescence photons with energies of around 10 keV (W-L and Cu-K), 60 keV (W-K_α) and 70 keV (W-K_β), which may reach the collecting volumes and contribute to the ionization charge. k_{dia} is obtained by two simulations, one with a nontransparent diaphragm (by defining a full absorption region) and another with the real diaphragm consisting of Densimet® D16. The correction is calculated as the ratio of the deposited energies in the collecting volume which result from the simulations of the nontransparent and real diaphragms.

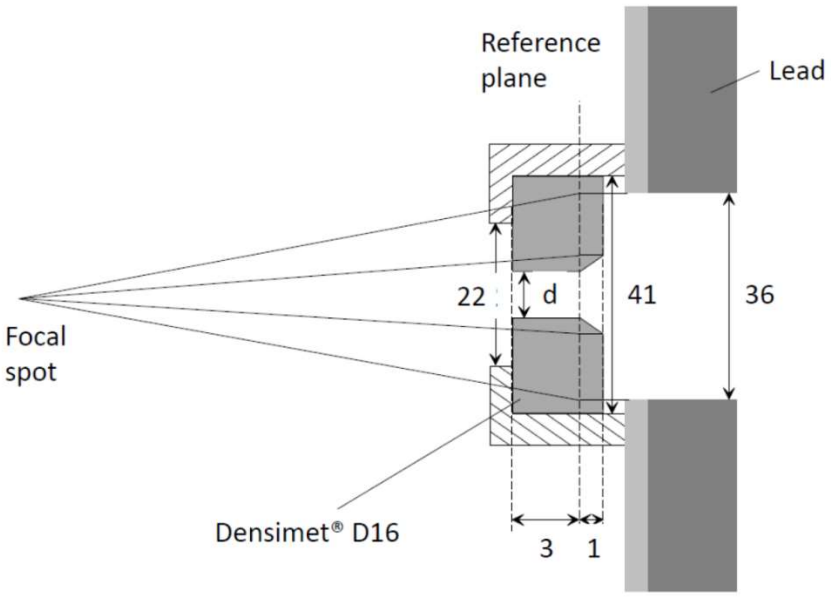

Figure 13. Schematic drawing of the diaphragm as used in the simulation with PK100M. The model was derived from the sketch shown in Figure 7. Dimensions are given in mm.

This correction is less than 1 because it corrects for an unwanted gain of the chamber signal. k_{dia} was calculated for all available aperture diameters and for two distances, 30 cm and 100 cm, between the focal spot and the reference plane. Results for the 6 mm and 20 mm diameter apertures are shown in Figure 14. The figures clearly show that the values of k_{dia} decrease (a) with increasing distance between the focus and the aperture (compare left and right diagrams), (b) with increasing aperture diameter (compare upper and lower diagrams) and (c) with increasing distance between the collecting volume and the aperture (compare MV1 to MV6 in each of the diagrams). These trends are expected because (a) with increasing distance between the focal spot and the aperture the divergency of the beam decreases and the photons pass the diaphragm edge with smaller angles of incidence; (b) the relative number of scattered photons on the edge of the aperture compared to the amount of primary photons which pass the inner part of the aperture without a hit decreases with the aperture diameter (i.e., the ratio of the perimeter to the area of a circle decreases proportionally to the inverse of the diameter); and (c) fewer scattered photons can reach the collecting volumes located further away from the source of scattered photons at the edge of the aperture.

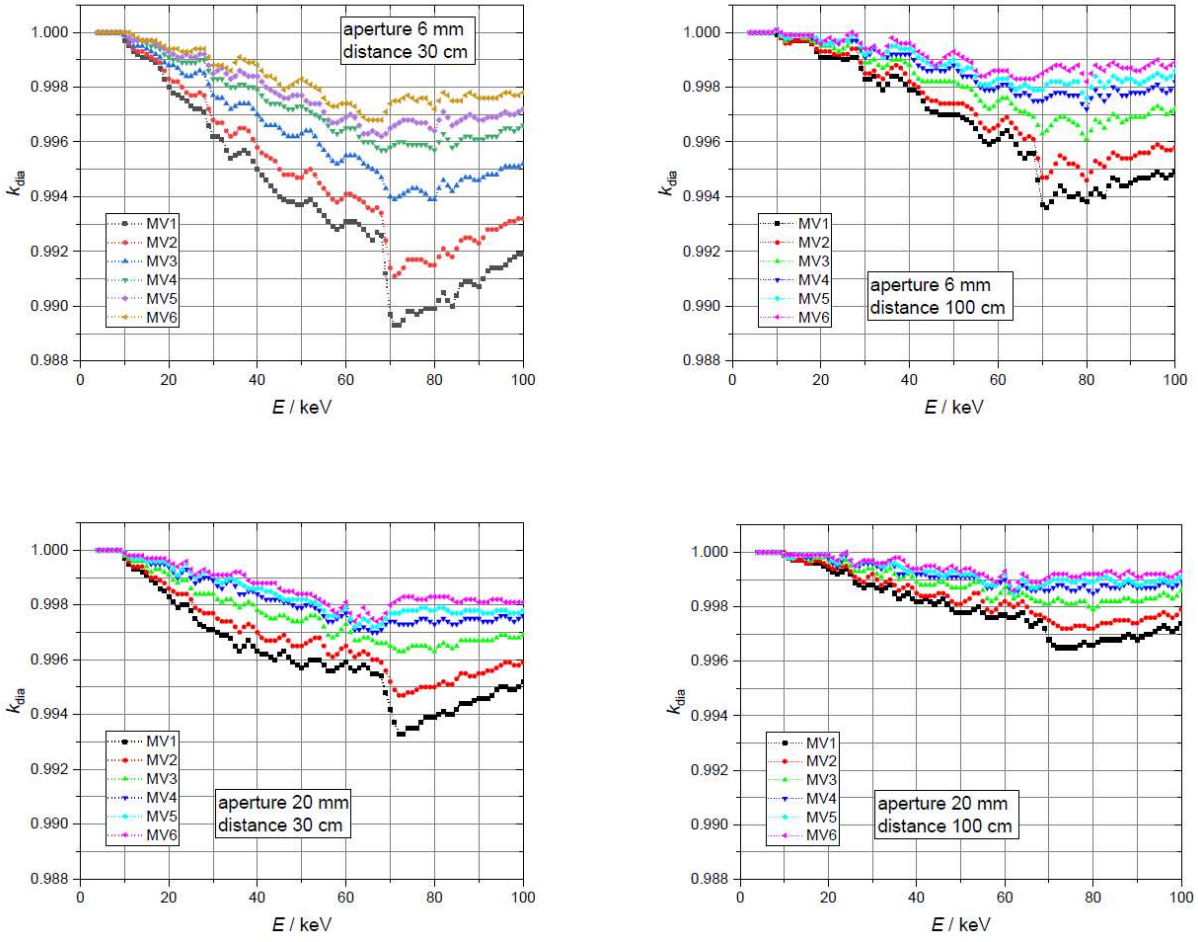

Figure 14. Correction $\boldsymbol{k_{\mathrm{dia}}}$ as a function of photon energy E for an aperture diameter of 6 mm (upper diagrams) and 20 mm (lower diagrams) at 30 cm (left diagrams) and 100 cm (right diagrams) distance between the focal spot and the reference plane of the aperture. Six curves are shown in each diagram which correspond to collecting volumes 1 (MV1) to 6 (MV6).

Finally, k_{dia} depends on the mass energy-attenuation coefficients of Densimet® (85% W, 15% Cu, density 16 g cm^{-3}) and thus on the photon energy. It was already mentioned that k_{dia} corrects for scattered (including fluorescence) and transmitted photons at the edge of the aperture. As an example, Figure 15 shows these contributions for primary photons of energy 30 keV, 60 keV and 100 keV, which are given quantitatively in Table 7. Note that the values of k_{dia} listed in the table relate to the values shown in the upper left diagram of Figure 14 for MV1.

The increase of the contributions from the W-*K* fluorescence photons for primary photon energies just above the K-edge of W (69.5 keV) are clearly visible in the curves shown in Figure 14.

Table 7. Relative air kerma contributions to k_{dia} from fluorescence and transmitted photons

Photon energy	Fluorescence photons	Transmitted photons	Sum	k_{dia}
30 keV	0.0032	0.0007	0.0039	0.9961
60 keV	0.0045	0.0025	0.0070	0.9930
100 keV	0.0072	0.0008	0.0080	0.9920

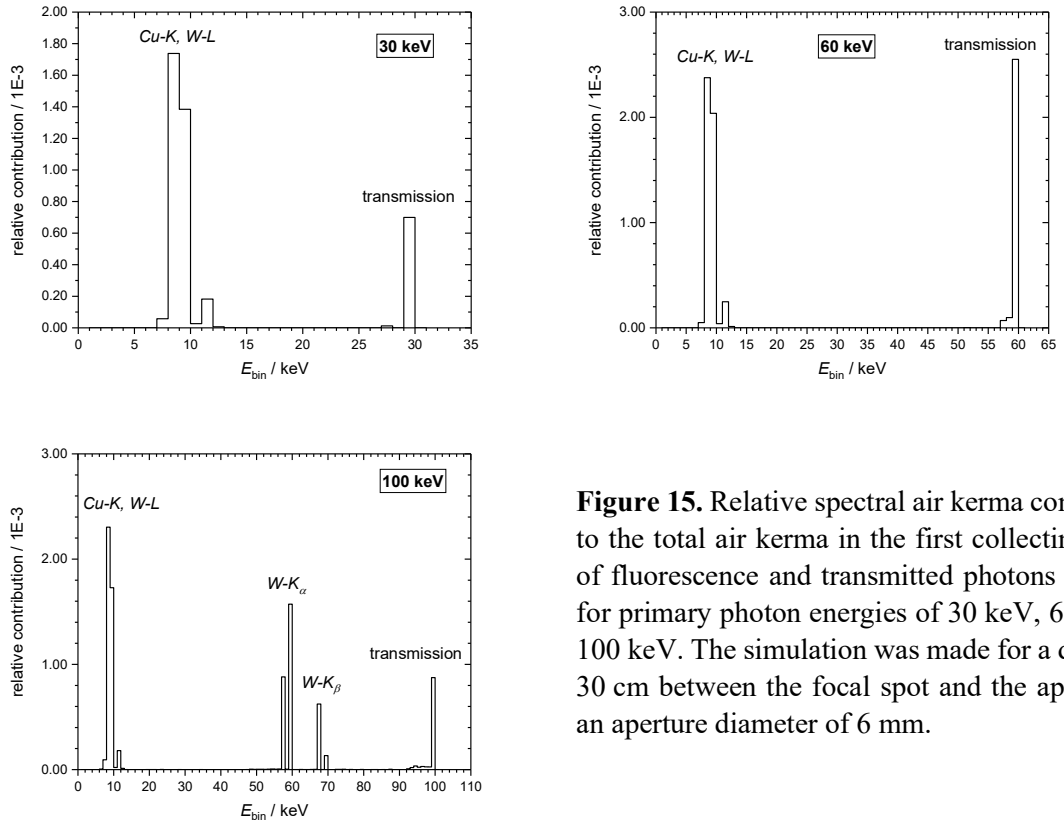

Figure 15. Relative spectral air kerma contributions to the total air kerma in the first collecting volume of fluorescence and transmitted photons calculated for primary photon energies of 30 keV, 60 keV and 100 keV. The simulation was made for a distance of 30 cm between the focal spot and the aperture and an aperture diameter of 6 mm.

Correction for scattered photons in the air of the PK100, k_{sc}

The correction k_{sc} was calculated by means of the PK100M simulation program. Two simulations were made, one with and one without the transport of air scattered photons. In the latter simulation, only the secondary electrons after the first interaction of the primary photons were transported, but not the scattered photons (fluorescence and Compton photons). Diaphragm effects were excluded by choosing a beam diameter equal to the aperture diameter. k_{sc} was obtained as the ratio of the deposited dose in the collecting region calculated without and with scattered photons. This ratio is less than one because the contribution from scattered photons increases the deposited dose. Figure 16 shows the results obtained in this way for k_{sc} as a function of monoenergetic photons in the range from 3 keV to 100 keV in steps of 1 keV. At 3 keV, $k_{\mathrm{sc}} = 0.9950$ is obtained, which changes significantly to 0.9830 at 4 keV. This large step is explained by the small amount of Ar atoms in the air, which is composed of the relative amounts of atoms by weight of 75.54% N, 23.18% O and 1.28% Ar. When the primary photon energy is above the K edge of Ar (3.2 keV), the excited Ar atoms emit fluorescence photons of about 3.2 keV, which increase the number of scattered photons at 4 keV compared to 3 keV and hence cause the observed change in k_{sc}. Above 4 keV, the probability for the photoelectric absorption by Ar atoms decreases, and above approximately 30 keV, k_{sc} is dominated by the effects of Compton scattered

photons. At higher photon energies, the mean free path of the scattered Compton photons increases and the probability that these will interact in the collecting volume decreases, which explains the asymptotic approach of k_{sc} to unity.

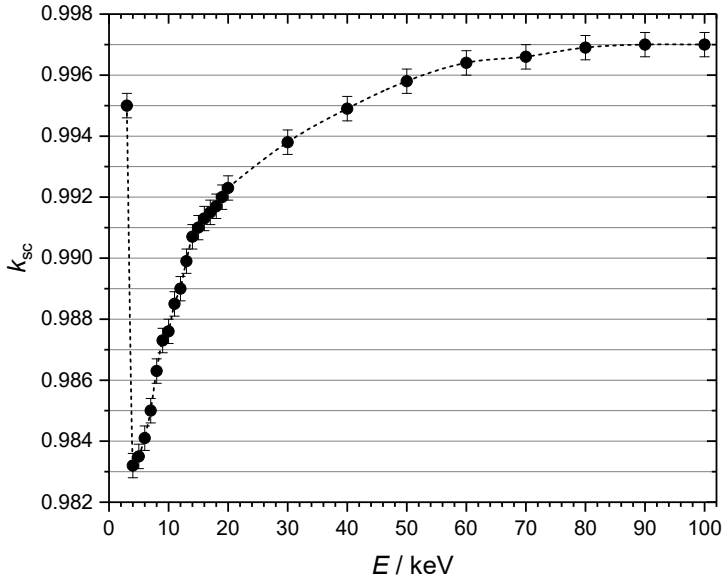

Figure 16. Correction factor $\boldsymbol{k_{sc}}$ as a function of the energy of the primary photons.

Correction for electron loss, k_e

A simulation with PK100M was made that excluded diaphragm effects and air attenuation. Only one photon interaction was allowed and only the secondary electrons were transported. The correction k_e was calculated as the ratio of the true value of the air kerma and the deposited dose in the collecting volume. The results obtained for photon energies up to 110 keV for the different collecting volumes (CVs) 1 to 6 are shown in Figure 17.

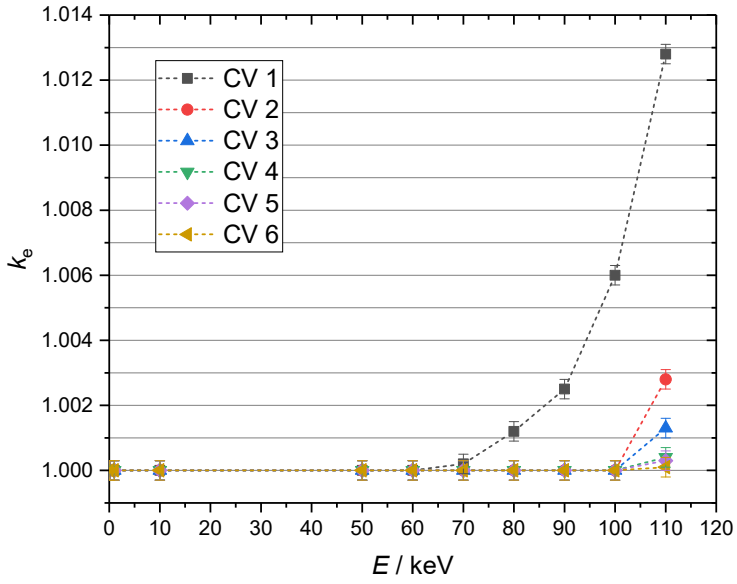

Figure 17. Correction factor k_e as a function of the energy of the primary photons.

There are two components contributing to k_e that are related to electron losses in the axial (in the direction of the primary beam) and radial directions. In the axial direction, an effect is observed which is related to a lack of secondary electron equilibrium (SEE). This effect causes k_e to begin rising in CV 1 at about 80 keV. Photoelectrons of kinetic energy 80 keV have a CSDA range in air of about 9 cm, which is already larger than the air path of 8.72 cm between the reference plane of the PK100 and the entrance plane of CV 1. For all other CVs, k_e is equal to 1 up to photon energies of 100 keV. The minimum distance to the planes that delimit the CVs in radial directions is about 12 cm, corresponding to a CSDA range of electrons in air with kinetic energies of about 95 keV. Therefore, it is unlikely that the paths of secondary electrons generated by primary photons up to 100 keV are limited by these planes, so the electron losses in radial directions will not contribute to k_e.

Product of correction factors, k

The product of correction factors *k* is defined as

$$k = k_{att}\, k_{ap} k_d k_{dia} k_{sc} k_e k_{iw} \tag{23}$$

One of the most frequently used configurations of the PK100 is the first collecting volume, an aperture of 20 mm diameter and a focus to reference plane distance of 100 cm. The factor *k* for this configuration is shown in Figure 18.

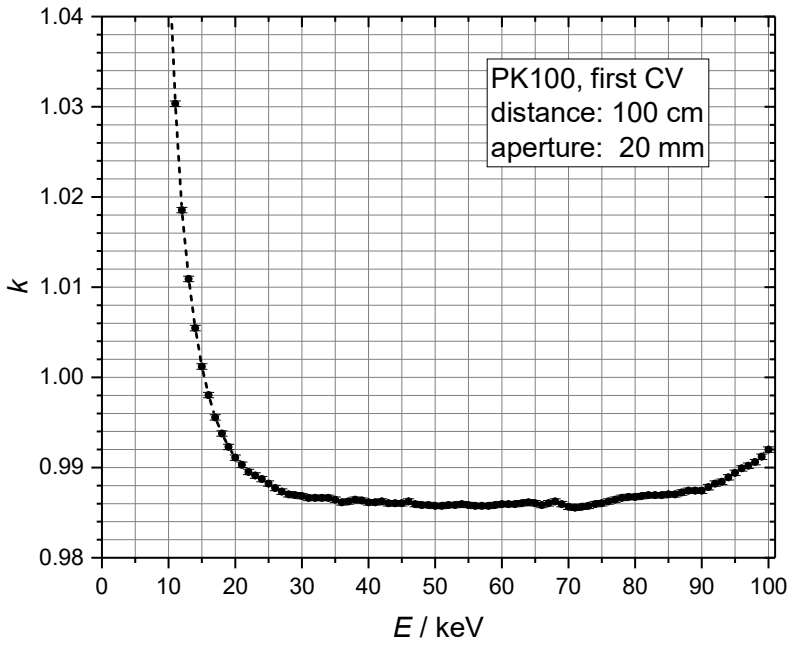

Figure 18. Product of all correction factors *k* calculated for the first collecting volume of the PK100, an aperture diameter of 20 mm and a focal spot to reference plane distance of 100 cm.

The figure clearly shows that *k* varies by no more than 0.2% in the photon energy range of 25 keV to 90 keV. The significant increase of *k* below 25 keV is caused by the air attenuation correction k_{att} (compare Figure 10). The moderate increase above 90 keV is caused by the lack of SEE in the first collecting volume, which is not the case in the other CVs because of larger air pathways.

4.1.4 Uncertainty of the air kerma rate determined with the PK100

The air kerma rate measured with the PK100 is obtained from the following equation:

$$\dot{K}_{\text{air}} = \frac{W_{\text{air}}}{e} \frac{I}{\varrho_{\text{air}} V} \frac{1}{1-\bar{g}} k_h k_{iw} k_{pol} k_s k_d k_p k_\rho k_{att}\, k_{ap} k_{dia} k_{sc} k_e \tag{24}$$

In practice, air kerma rates are measured for defined reference x-radiation qualities. The PK100 is well suited for radiation qualities generated with tube voltages in the 7.5 kV to 100 kV range. The correction factors for x-radiation qualities characterized by their photon fluence spectra ϕ_E with maximum energies E_{max} are obtained as the air-kerma-weighted mean values $\bar{k}$ according to [20]:

$$\bar{k} = \frac{\int_0^{E_{max}} k(E) \frac{\mu_{tr}}{\varrho_{air}} E\phi(E) dE}{\int_0^{E_{max}} \frac{\mu_{tr}}{\rho_{air}} E\phi(E) dE} \tag{25}$$

The uncertainty budget shown in Table 8 was estimated for a quality generated with a W-anode tube at 25 kV and filtered with 0.374 mm Al (CCRI recommended quality for key comparisons [21], characterized by an aluminium half-value layer of 0.24 mm). The photon fluence spectrum is shown in Figure **19**.

Table 8. Uncertainty budget estimated for the radiation quality CCRI 25 kV [22]

Parameter	Description	Value	u_{iA} (%)	u_{iB} (%)	u_{i} (%)
W_{air}/e	Mean energy (eV)	33.97		0.35	0.35
I	Ionization current	-	0.10	0.06	0.12
ρ_{air}	Air density (kg m^{-3})	1.2048		0.01	0.01
V	Collecting volume (mm^3)	1575	0.06		0.06
$1/(1-\bar{g})$	Radiative loss correction	1.0000		0.01	0.01
k_h	Humidity	0.9980		0.03	0.03
k_{iw}	$= k_{\text{ii}} k_{\text{W}}$ (section 3.2)	0.9968		0.11	0.11
k_{pol}	Polarity	1.0000	0.05	0.05	0.07
k_s [1)]	Saturation	1.0022	0.05	0.05	0.07
k_d	Field distortion	0.9910	0.10		0.10
k_p	Wall penetration	1.0000	0.05		0.05
k_ρ	Air density correction	1.0000	0.036		0.036
k_{att}	Air attenuation	1.0310	0.05	0.05	0.07
k_{ap}	Guard strip attenuation	1.0060	0.05		0.05
k_{dia}	Diaphragm effects	0.9996		0.05	0.05
k_{sc}	Scattered radiation	0.9902		0.05	0.05
k_e	Electron loss	1.0000		0.05	0.05
$\dot{K}_{\text{air}}$	Air kerma rate (result)	-	0.19	0.39	0.44

[1)] Calculated for the air kerma rate 1 mGy/s

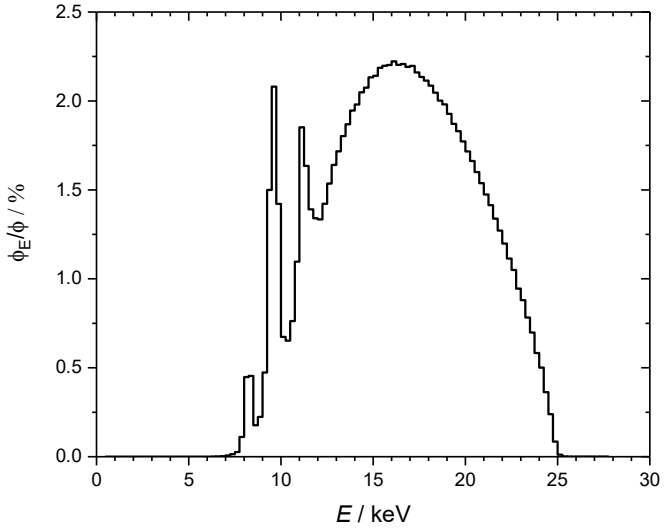

Figure 19. Normalized photon fluence spectrum ϕ_E/ϕ of the CCRI 25 kV radiation quality.

The largest uncertainty component is caused by the uncertainty of the value of W_{air}/e, without which the remaining uncertainties add up to 0.27%. When two primary free-air chambers are compared to one another, both will use the same value and uncertainty of W_{air}/e, meaning that this large uncertainty component will cancel out.

4.2 Cylindrical free-air chamber FK ("Fasskammer")

The "**F**ass**k**ammer" (FK) is a cylindrical-type free-air chamber and is used for x-radiation qualities generated with tube voltages in the 30 kV – 300 kV range. The chamber was conceived, designed and manufactured at PTB and completed as early as 1951. Since then, it has been used as the primary standard for the determination of the quantity exposure/air kerma.

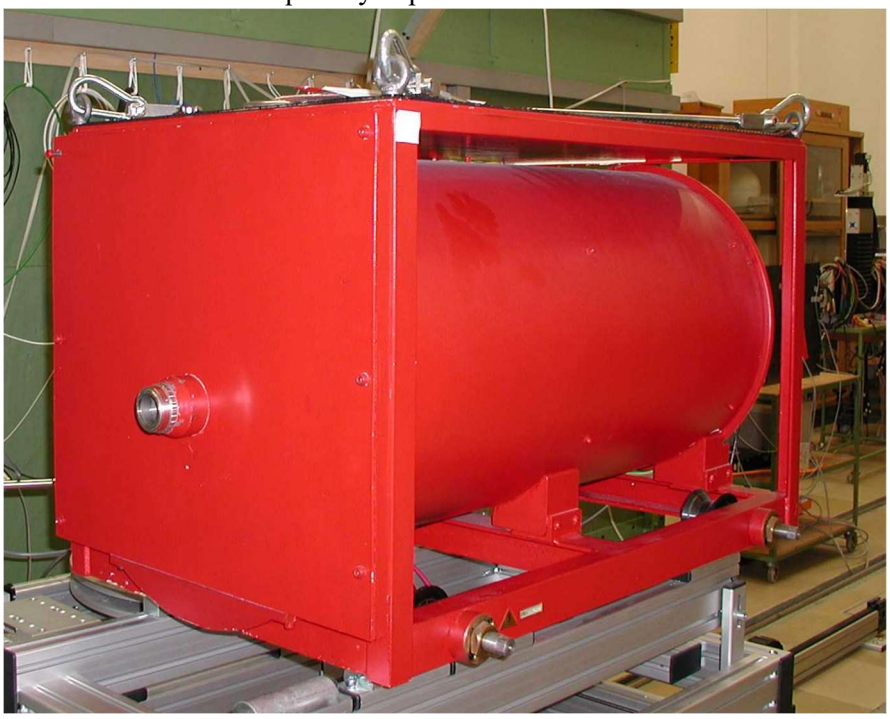

Figure 20. Photo of the free-air chamber type FK.

4.2.1 Design and dimensions

A schematic overall view of the chamber is shown in Figure 21. The chamber consists of a rod-shaped central electrode located on the central axis of a cylindrical high voltage electrode (E_{HV}) which is surrounded by the cylindrical chamber housing (H). The circular aperture (AP) is located with its midpoint 45 mm below the central axis of the cylindrical chamber. The x-ray beam enters the chamber through the aperture such that the beam axis runs parallel to the central electrode at a distance of 45 mm. The x-ray beam leaves the chamber through a circular hole at the rear end of the chamber, which is sealed by a thin 0.05 mm polyethylene (PE) foil. This minimizes backscattering at the rear end.

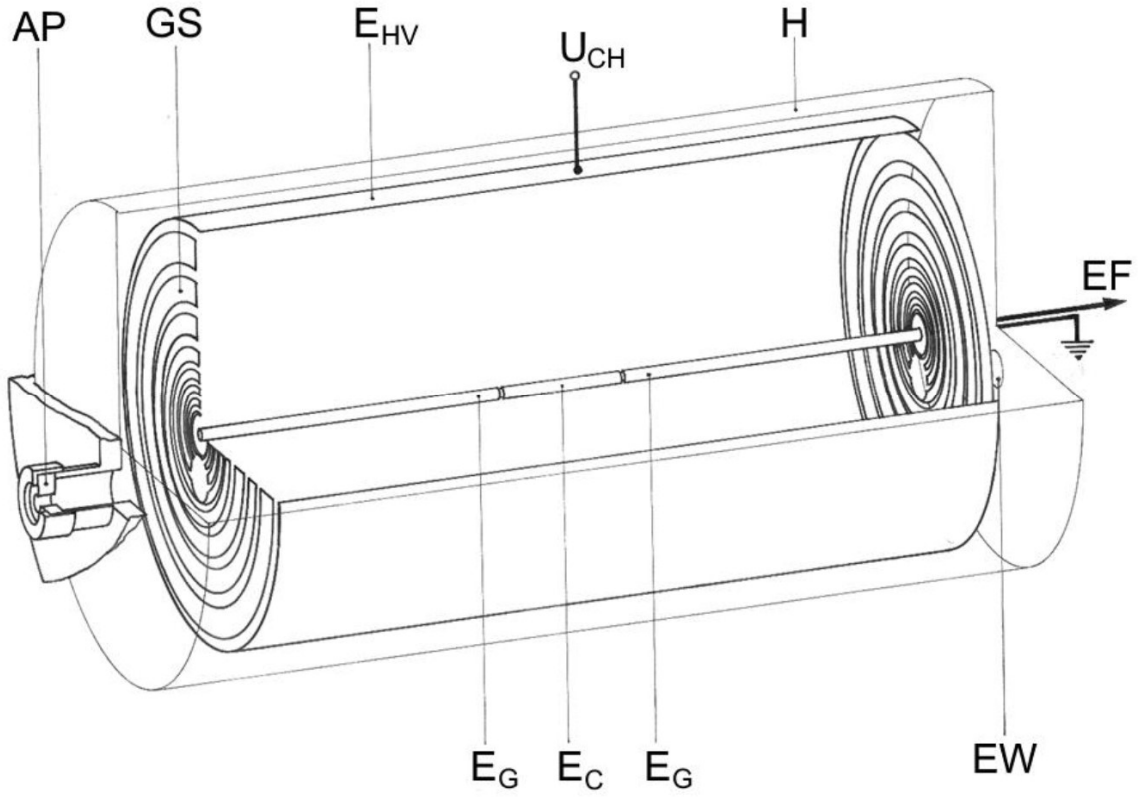

AP	Aperture
GS	Guard strip
E_{HV}	High voltage electrode
E_G	Guard electrode
E_C	Collecting electrode
H	Housing
U_{CH}	Chamber high voltage
EW	Exit window
EF	Electrometer feed

Figure 21. Schematic overall view the FK.

The central electrode is made of an aluminium tube with an outer diameter of 7 mm. The middle section is electrically isolated from the remaining sections by inserts of polished Trolitul® as shown in Figure **22** and forms the collecting electrode (E_C). The remaining sections on either side serve as guard electrodes (E_G). The length of the entire central electrode system is 71.4 cm. It can be easily replaced by other central electrode systems with collecting electrodes of different lengths ranging from 5 cm to 25 cm. The centre of the collecting electrodes is always at the same position in the chamber. The counter electrode (E_{HV}) is a cylinder made of 2 mm thick aluminium sheet and has an inner diameter of 40 cm.

The inner surface of the cylinder is covered with a 0.2 mm layer of graphite. The high voltage electrode is connected to 3000 V and the guard electrodes are grounded. A slight potential difference of up to approximately 1 mV may exist between the collecting electrode and the guard. This is caused by the input amplifier of the electrometer.

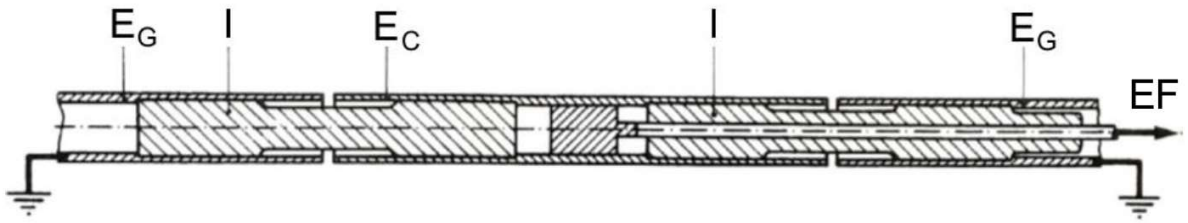

Figure 22. Schematic drawing of the central electrode.

E_G Guard electrode
E_C Collecting electrode
I Isolator (Trolitul®)
EF Electrometer feed

Electrical field distortions between the central and high voltage electrodes caused by edge effects are minimized by the guard electrodes and by 8 annular guard strips at the insides of the chamber's front and back walls. The widths of the annular guard strips correspond to the logarithmic decrease of the electrical field strength between the central and outer electrodes in the radial direction. The annular guard strips consist of graphitized aluminium which are electrically connected via the resistors of a voltage divider. Each resistor has a resistance of 4 MΩ. The guard strips have circular radiation entrance and exit openings of diameter 45 mm.

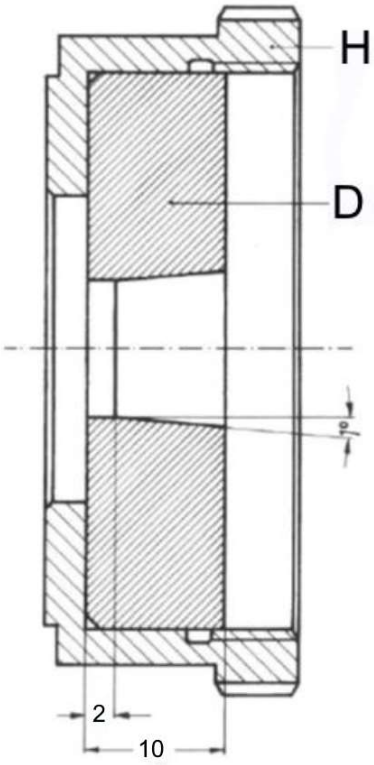

Figure 23. Technical drawing of the diaphragm of the FK. H: Holder, D16: Diaphragm body made of Densimet®.

The chamber housing at the radiation entrance side is covered with a lead layer of thickness 22 mm. The cylindrical side wall is covered with a 2 mm lead coat to attenuate stray radiation that hits the chamber. An additional lead shield for the back wall of the chamber is not necessary. If there is still some radiation penetrating the chamber walls and contributing to the signal, it is measured and corrected for as described above in section 3.2.

The diaphragm (see Figure 23 on the left) consists of the holder H and the diaphragm body made of Densimet® D16, which is a tungsten-copper alloy (85% W, 15% Cu) of density 16 g cm^{-3}. The outer diameter and thickness of the diaphragm body are 41 mm and 10 mm, respectively. The first 2 mm section of the aperture is cylindrical and the remaining 8 mm section is conical with an opening angle of 1°. The diaphragm holder is constructed such that the whole assembly can be easily exchanged with another having a different aperture diameter. Five different apertures are available with nominal circular diameters of 8, 10, 15, 20 and 30 mm.

The measuring volume of the chamber is given by the cylinder which has the diameter of the aperture and the effective width w_{eff} of the collecting electrode. The latter is given by the width of the collector plus half the widths of the insulating gaps on both sides of the central collecting electrode (Figure 21). The reference point of the chamber where the air kerma rate is measured is located on the axis of the aperture at the point where the cylindrical shape transits to the conical one. The distance between the reference point of the

chamber and the centre of the collecting electrode is 481 mm. The actual geometrical data of the chamber are given in Table 9 and Table 10.

Table 9. Main dimensions of the cylindrical free-air ionization chamber FK

Item	Dimension
Inner diameter of the high voltage electrode (E_{HV})	400 mm
Outer diameter of the central electrode (Figure 2)	7 mm
Distance between the central electrode axis and the beam axis	45 mm
Length of the collecting electrodes	See Table 2
Distance between the guard strips at the front and the back (Figure 1)	718 mm
Outer diameter of the diaphragm	41 mm
Thickness of the diaphragm	10.0 mm
Thickness of the lead shield at the front of the housing	20 mm
Thickness of the lead shield around the housing (except front wall)	2 mm
Air path *A* between the reference point in the aperture and the centre	481 mm

Table 10. Measuring volumes of the cylindrical free-air ionization chamber FK

Collecting electrodes		Apertures				
Nom.	w_{eff} (cm)	0.8 b	1.0 b	1.5 b	2.0 b	3.0 b
length		Diameter (cm)				
		0.8004	1.0016	1.5008	2.0009	3.0066
		Measuring volumes (cm^3)				
5	5.0090	2.5203	3.9465	8.8607	15.7509	35.5632
10	10.0141	5.0387	7.8900	17.7145	31.4895	71.0987
15	15.0043	7.5495	11.8217	26.5420	47.1812	106.5284
20	20.0009	10.0636	15.7584	35.3808	62.8931	142.0036
25	25.0989	12.6287	19.7751	44.3990	78.9239	178.1988

4.2.2 Chamber model for Monte Carlo simulations

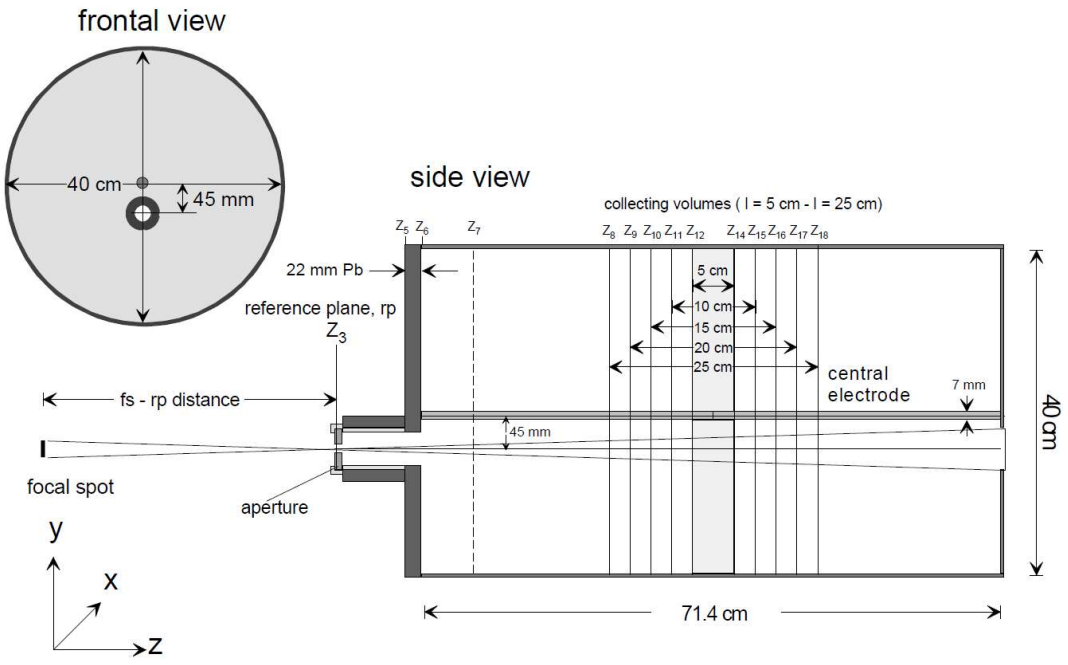

Figure 24. Sketch of the geometry of the FK as used in the EGS4-based user code "FKM".

The transport of x-rays through the FK was simulated with the Monte Carlo code system EGS4 [10] as described in section 3.3. The EGS4-based user code designated "FKM" was developed for this purpose. The geometrical model used for the simulation is shown in Figure 24. FKM allows the calculation of the correction factors k_{sc} , k_{e}, k_{dia} and k_{cpe} described in section 3, as well as the correction for the effects induced by the central electrode, designated k_{sh}. Details of the calculation methods and the results for each correction factor will be given in the following section.

4.2.3 Correction factors for the FK

Correction for lack of saturation, k_{s}

Saturation effects were measured according to the methods described in 3.2. The correction for initial recombination was found to be k_{si}=1.00092. The volume recombination was estimated as

$$k_{\mathrm{SV}} = 1 + \frac{R_V}{U^2} I_{FK} \tag{26}$$

where R_V = 1.15 *10^{13} V^2/A, U is the polarizing voltage and I_{FK} is the chamber current.

The validity of k_{SV} according to eq. (26) was confirmed experimentally by the following method. The FK was positioned at PTB's x-ray calibration facility at a fixed distance from the x-ray tube. For a selected x-radiation quality, the saturation-corrected ionization current of the FK was measured at different x-ray tube currents, causing the ionization current of the FK to vary from 0.3 nA to 3 nA and the k_{SV} to vary between 1.001 and 1.005. The saturation-corrected ionization current of the FK was then normalized to the ionization current of the transmission monitor chamber which is always used at the calibration facility and which can be assumed to be characterized by a negligible saturation loss in this ionization current range. The suitability of eq. (19) to determine k_{SV} was confirmed by the fact that the normalization factor remains constant within the uncertainty of the measurements (approximately 0.1%) for all tube currents between 1 mA and 30 mA.

Correction for electrical field distortion, k_{d}

The special guard strip design described in 4.2.1 minimizes the distortion of the electrical field at the insides of the front and back edges of the cylindrical capacitor. From the design it can be assumed that there is only a negligibly small distortion at the innermost collecting volume obtained if the shortest central measuring electrode (5 cm nominal length) is installed and k_{d} = 1 applies. To obtain the potential influences of distortions for the other collecting volumes with central electrodes having nominal lengths of 10 cm, 15 cm, 20 cm and 25 cm (and which are hence increasingly closer to the edges of the cylindrical capacitor), the ratio $I(L) / L$ was measured at a fixed radiation quality and constant tube current, where $I(L)$ is the corrected ionization current measured with the electrode of length L. It turned out that this ratio was almost constant within the estimated relative uncertainty of the measurements (approximately 0.1%). Thus, k_{d} = 1.000 with a relative uncertainty of 0.1% is used for all central electrodes.

Correction for air attenuation between reference and measuring point, k_{att}

The air attenuation correction, k_{att}, along the air path A = 48.1 cm was calculated as a function of monoenergetic photons according to eq. (20). The results are shown in Figure 25. Given the steep increase of k_{att} below about 30 keV, it does not make sense to use the FK free-air chamber at radiation qualities which are generated with x-ray tube high voltages of less than 30 kV.

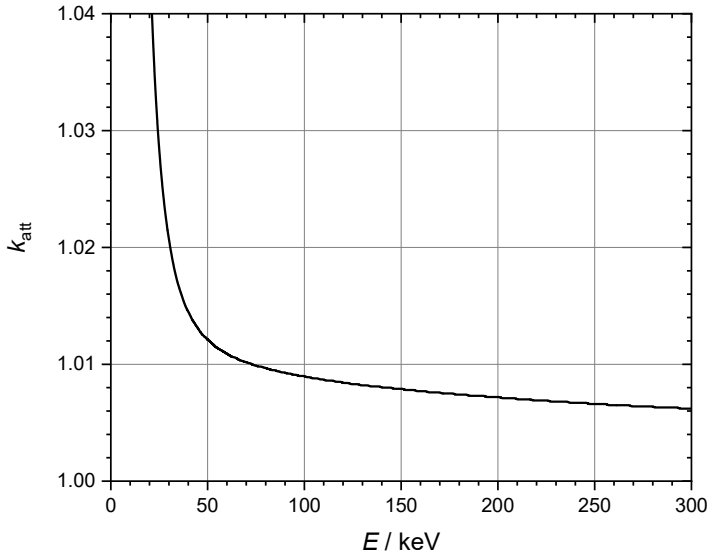

Figure 25. Air attenuation correction $\boldsymbol{k_{att}}$ calculated for the FK according to eq. (20) along the air path length A = 48.1 cm.

Correction for diaphragm effects, k_{dia}

The model of the diaphragm used in the FKM Monte Carlo simulation is shown in Figure 26. The transmission through the 10 mm thick body of the diaphragm made of Densimet® D16 for photons of energies 200 keV and 300 keV is estimated as 0.0017% and 1.06%, respectively. The correction for transmitted photons can therefore not be neglected for photons with energies above 200 keV. About 8 cm away from the first aperture there is a second one with a diameter of 37 mm, as shown the figure.

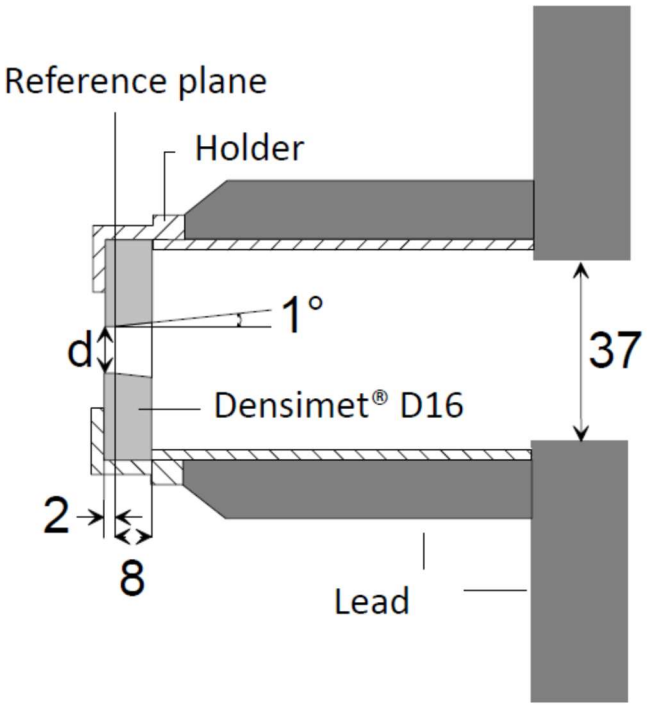

Figure 26. Schematic drawing of the diaphragm as used in the simulation with FKM. The model was derived from the sketch shown in Figure 23. Dimensions are given in mm.

This second aperture is larger than the first one, which can have a maximum diameter of 30 mm as described above. Primary photons which pass through the first aperture will also pass through the second one, but scattered photons from the edge of the first aperture will most likely be absorbed by the second aperture edge. The correction k_{dia} is obtained by two simulations with the user code FKM, one with a nontransparent diaphragm body (by defining a full absorption region around the aperture) and another with the real diaphragm body consisting of Densimet® D16. The correction is calculated as the ratio of the deposited energies in the collecting volume which result from the simulations of the nontransparent and real diaphragms. The results are shown in Figure 27.

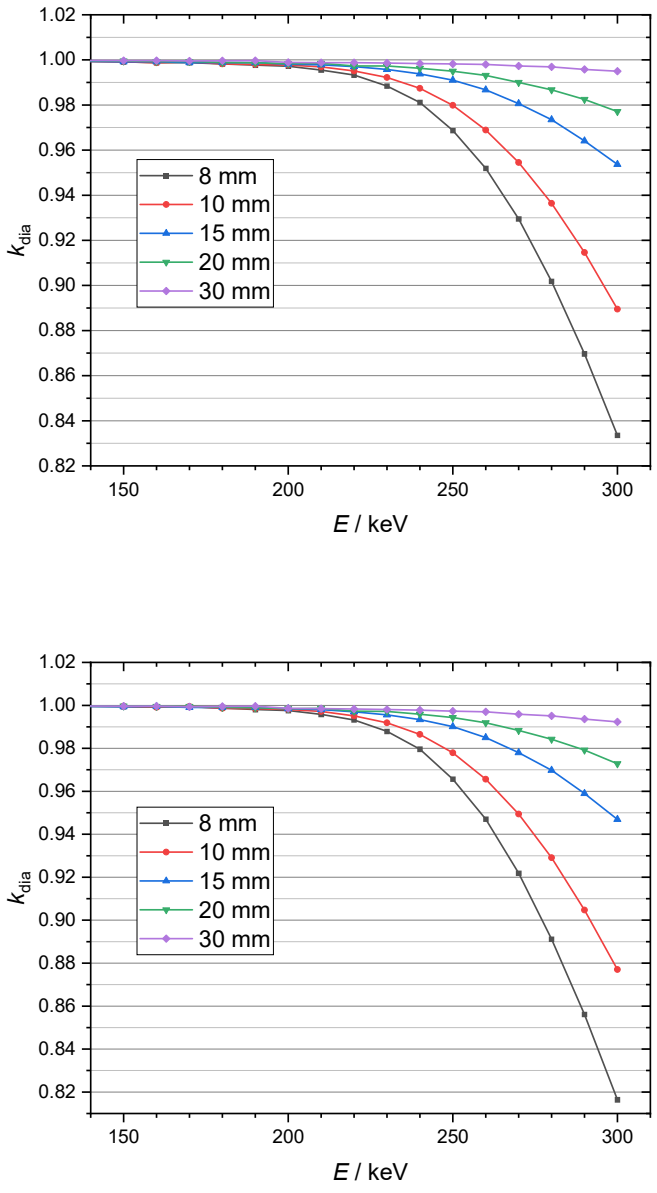

Figure 27. Correction factor k_{dia} calculated as a function of photo energy for aperture diameters 8 mm to 30 mm with a distance of 1 m (upper diagram) and 3 m (lower diagram) between the reference plane and the x-ray focus.

The correction k_{dia} becomes significant above 200 keV and is largest at 300 keV. It decreases with increasing aperture diameters because the fraction of photons transmitted through the diaphragm body to those passing through the aperture decreases. Corrections at 3 m distance are slightly larger than the

corresponding values at 1 m because the divergence of the beam decreases with increasing distance from the source and thus the path lengths of the photons through the diaphragm body are shorter.

Correction for effects induced by the central electrode, k_{sh}

The x-ray beam enters the chamber through the aperture such that the beam axis runs parallel to the central electrode at a distance of 45 mm and leaves the chamber through a circular hole at the rear end of the chamber (see Figure 24). Some of the secondary electrons generated by primary photon interactions get absorbed by the 7 mm diameter central electrode before they can finish their free path lengths in air. This leads to a loss of ion pairs that would otherwise be created along the path of the electrons through the collecting volume of the chamber. This kind of electron absorption can be described as a central electrode shadow effect, so the correction factor for this effect was named k_{sh}. It corrects for a loss of ion pairs and thus its value is greater than 1. The correction was calculated with the FKM simulation code according to the principles explained in section 3.3. To find the correction k_{sh} separated from the other perturbation effects, these were eliminated by the following settings. The beam diameter in the reference plane was set equal to the corresponding aperture diameter. Only one interaction was allowed for primary photons and only electrons were transported. The diameter of the outer electrode was set to 50 cm. This eliminated the effects due to the diaphragm, path length limitations of the electrons by the outer electrode, and air scattered photons. The resulting correction factors k_{sh} for the 8 mm and 30 mm aperture diameters are shown in Figure 28 as a function of the photon energy.

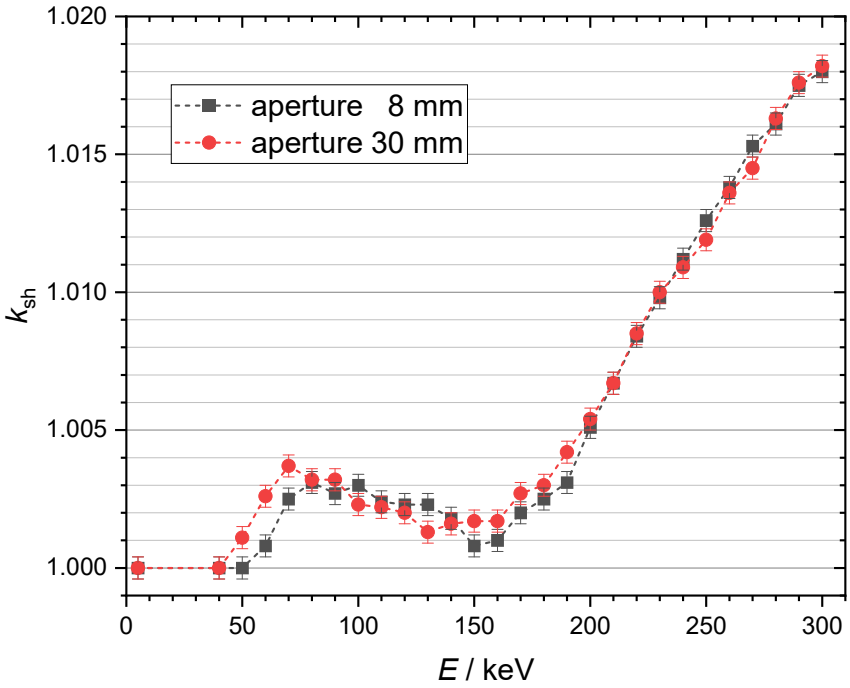

Figure 28. Correction factor k_{sh} as a function of the photon energy calculated for apertures of diameter 8 mm and 30 mm.

Up to photon energies of 40 keV for the larger or 50 keV for the smaller aperture, the kinetic electron energy is not sufficient to reach the central electrode and thus the correction is 1. Above these energies, electrons can begin reaching the central electrode and can get absorbed. The correction k_{sh} is proportional to the kinetic energy and hence to the path length in air of the secondary electrons. Thus, k_{sh} increases up to a local maximum value of around 70 keV for the larger and 90 keV for the smaller aperture. Due

to the decreasing probability of the photoelectric effect and the corresponding increase of the Compton effect, the correction factor starts to decrease because the Compton electrons have less kinetic energy than the photoelectrons. A local minimum is observed at about 150 keV, where the photoelectric effect is less likely and photon interactions are dominated by Compton scattering. Due to the increase in the kinetic energy of the Compton electrons that occurs with increasing photon energy, k_{sh} rises steeply until a value of 1.018 is reached at 300 keV.

Correction for scattered photons in the air of the FK, k_{sc}

The correction k_{sc} was calculated by means of the FKM simulation program. Two simulations were made, one with and one without the transport of air scattered photons. In the latter simulation, only the secondary electrons after the first interaction of the primary photons were transported, but not the scattered photons (fluorescence and Compton photons). Diaphragm effects were excluded by choosing a beam diameter equal to the aperture diameter. k_{sc} was obtained as the ratio of the deposited dose in the collecting region calculated without and with scattered photons. This ratio is less than one because the contribution from scattered photons increases the deposited dose. Figure 29 shows the results obtained in this way for k_{sc} as a function of monoenergetic photons in the range from 5 keV to 300 keV. The interpretation of the curve corresponds to that of the PK100 (Figure 16).

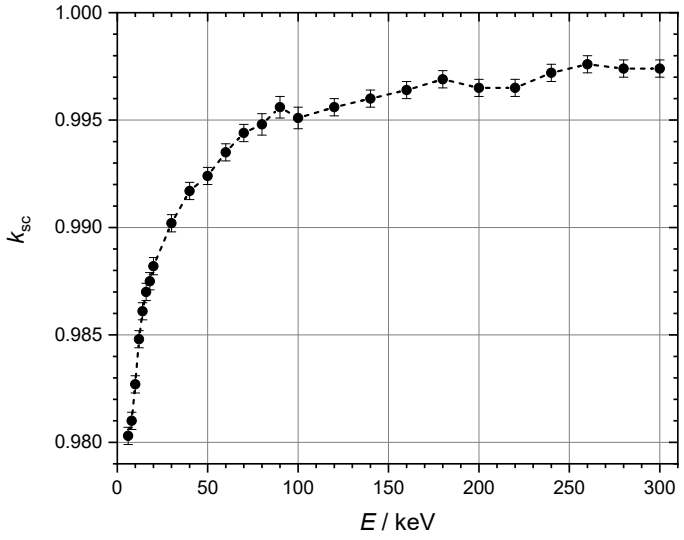

Figure 29. Correction factor k_{sc} calculated as a function of the photon energy.

Correction for electron loss, k_e

A simulation with FKM was made without the presence of a central electrode and where diaphragm effects and air attenuation were excluded. Only one photon interaction was allowed and only the secondary electrons were transported. The correction k_e was calculated as the ratio of the true value of the air kerma and the deposited dose in the collecting volume under these conditions. The relative statistical uncertainty was less than 0.02%. The results obtained for photon energies up to 300 keV are shown in Figure 30 for aperture diameters 8 mm and 30 mm. The CSDA range in air of secondary electrons generated by primary photons of energies up to about 120 keV is less than 20 cm, which is equivalent to the radius of the outer electrode of the cylindrical FK. These electrons lose their entire kinetic energy in the air of the chamber and so k_e is equal to 1. Above 120 keV, the secondary electron range in air increases to values greater than 20 cm and the electrons get absorbed by the outer electrode

before they finish their path through the air, causing k_e to begin rising to a photon energy of about 200 keV, where a local maximum is observed. A further increase in the photon energy causes a decrease of k_e because the photoelectric effect cross section decreases, and the Compton effect cross section increases. The Compton electrons have lower kinetic energies than do the photoelectrons, which explains the decrease of k_e to around 250 keV, where a local minimum is observed. A further increase in the photon energy up to 300 keV causes a significant increase of k_e with increasing kinetic energies of the Compton electrons. There is only a slight difference between the curves calculated for the smallest (8 mm) and largest (30 mm) aperture diameters.

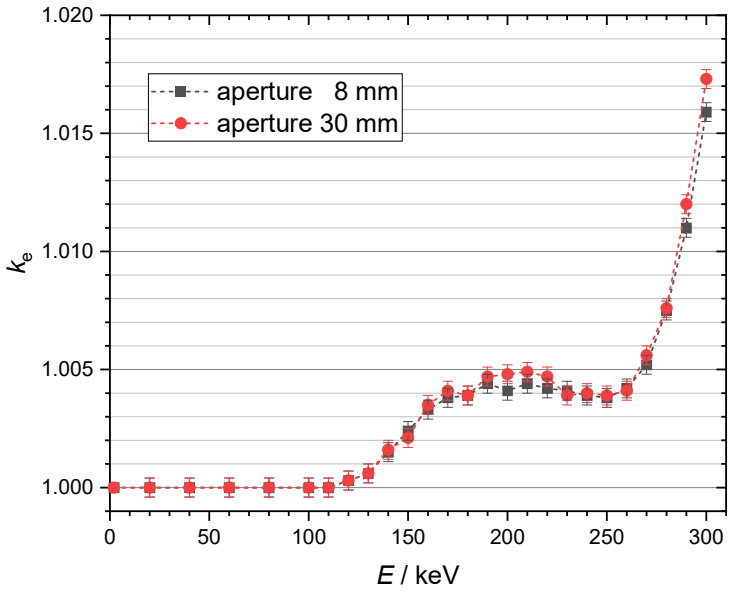

Figure 30. Correction factor k_e as a function of the photon energy calculated for apertures of diameter 8 mm and 30 mm.

Product of correction factors, k

The product of correction factors k is defined as

$$k = k_{att}\, k_{sh} k_d k_{dia} k_{sc} k_e k_{iw} \tag{27}$$

Figure 31 shows the product of the correction factors as a function of the energy of the primary photons. The curves shown in the upper diagram were calculated for the measuring volume with a measuring electrode length of 5 cm and apply to a focus-reference distance of 100 cm and to the aperture diameters of 1.0 cm to 5.0 cm. Below 30 keV, the curves rise steeply due to the significant increase in air attenuation here. From 30 keV to about 220 keV, the curves remain at a nearly constant level close to 1.01 before branching out at higher energies to higher or lower values depending on the aperture diameter. This behaviour can be explained by the strong increase of the correction factor for the path length limitation of the secondary electrons k_e above 220 keV (Figure 30) with a simultaneous strong decrease of the correction factor for the aperture edge transmission k_{dia} (Figure 27), which weakens as the diameter of the aperture becomes larger. At an aperture diameter of 0.8 cm, the correction factor k_{dia} dominates, causing the curve to fall, while at an aperture diameter of 3.0 cm, the correction factor k_e dominates, causing the curve to rise. At the aperture diameter of 1.5 cm, these two opposing contributions almost offset one another. The lower diagram of Figure 31 shows separately the part of the curve for the 1.5 cm aperture diameter within a scale of 0.99 and 1.03. The energy range for which the FK can reliably be used as a primary standard for air kerma measurements can be read from the diagram. For energies below 30 keV, the correction factors for air attenuation increase steeply.

Therefore, larger uncertainties must be expected when using the chamber for generating voltages below 30 kV. *k* varies by no more than about 0.7% between 30 keV and 270 keV, which qualifies this chamber for air kerma measurements in this energy region. For the apertures greater than 10 mm, the FK can be used for x-ray qualities with generating voltages up to 300 kV.

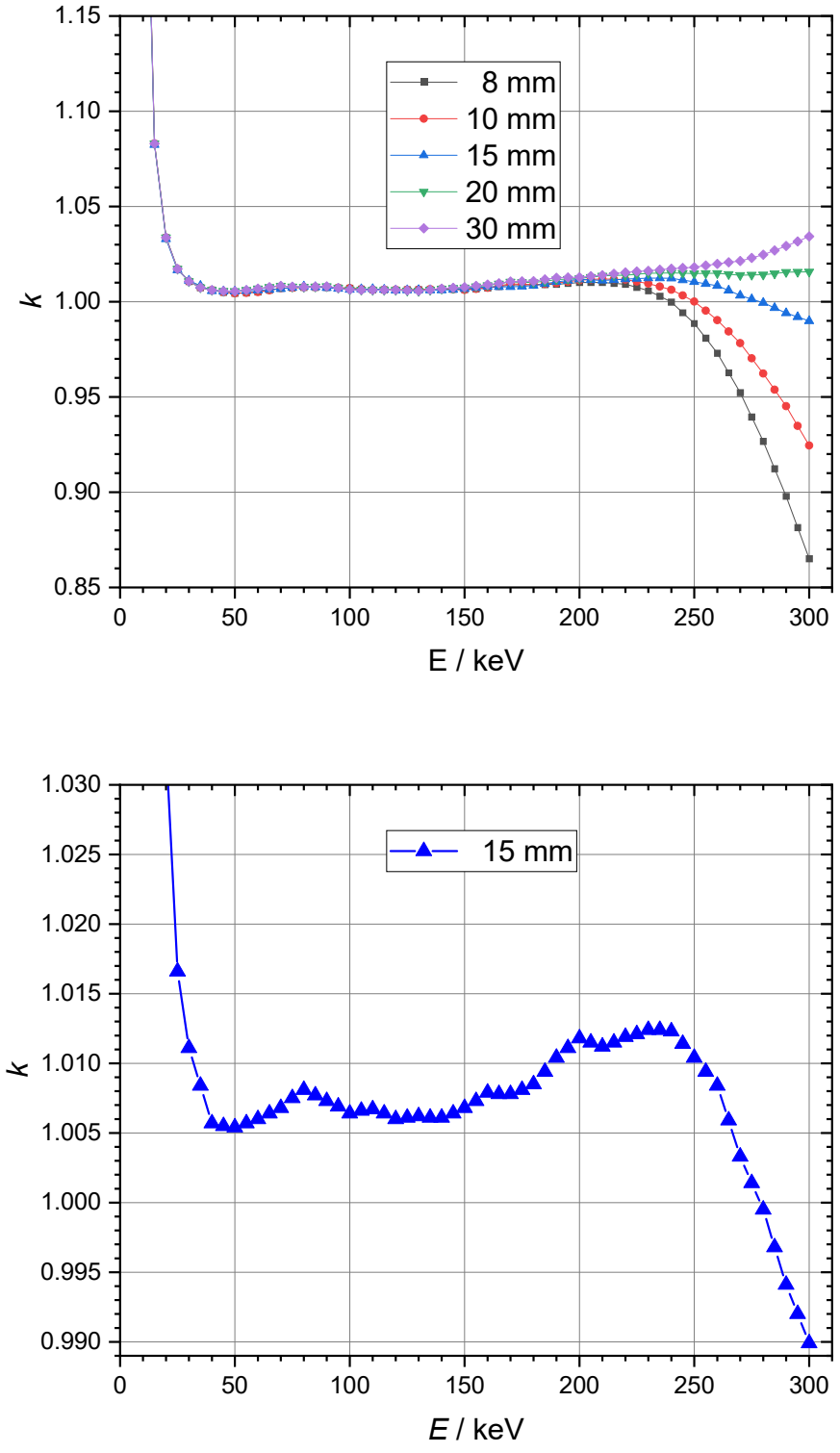

Figure 31. Product of all correction factors *k* calculated for the 5 cm collector electrode of the FK and all available apertures (upper diagram) and for the aperture of diameter 15 mm with enlarged scale (lower diagram) at a focal spot to reference plane distance of 100 cm.

4.2.4 Uncertainty of the air kerma rate determined with the FK

The air kerma rate measured with the FK is obtained from the following equation:

$$\dot{K}_{\text{air}} = \frac{W_{\text{air}}}{e} \frac{I}{\varrho_{\text{air}} V} \frac{1}{1-\bar{g}} k_h k_{iw} k_{pol} k_s k_d k_p k_\rho k_{att}\, k_{sh} k_{dia} k_{sc} k_e \qquad (28)$$

In practice, air kerma rates are measured for defined reference x-radiation qualities. The FK is well suited for radiation qualities generated with tube voltages in the 30 kV to 300 kV range. The correction factors for x-radiation qualities characterized by their photon fluence spectra ϕ_E with maximum energies E_{max} are obtained as the air-kerma-weighted mean values $\bar{k}$ according to eq. (25).

Table 11. Uncertainty budget estimated for the radiation quality CCRI 250 kV [23]

Parameter	Description	Value	u_{iA} (%)	u_{iB} (%)	u_{i} (%)
W_{air}/e	Mean energy (eV)	33.97		0.35	0.35
I	Ionization current	-	0.10	0.06	0.12
ρ_{air}	Air density (kg m^{-3})	1.2048		0.01	0.01
V	Collecting volume (mm^3)	15759	0.05		0.05
$1/(1-\bar{g})$	Radiative loss correction	1.0003		0.02	0.02
k_h	Humidity	0.9980		0.04	0.04
k_{iw}	$= k_{\text{ii}} k_{\text{W}}$ (section 3.2)	0.9968		0.11	0.11
k_{pol}	Polarity	1.0000	0.05		0.05
k_s [1)]	Saturation	1.0013	0.05		0.05
k_d	Field distortion	1.0000		0.10	0.10
k_p	Wall penetration	1.0000	0.05		0.05
k_ρ	Air density correction	1.0000	0.036		0.036
k_{att}	Air attenuation	1.0083		0.05	0.05
k_{sh}	Shadow effect (c.e.)	1.0029		0.05	0.05
k_{dia}	Diaphragm effects	0.9988		0.05	0.05
k_{sc}	Scattered radiation	0.9958		0.05	0.05
k_e	Electron loss	1.0019		0.05	0.05
$\dot{K}_{\text{air}}$	Air kerma rate (result)	-	0.19	0.39	0.43

[1)] Calculated for the air kerma rate 0.5 mGy/s

The uncertainty budget shown in Table 11 was estimated for a quality generated with a W-anode tube at 250 kV and filtered with 2.302 mm Al (CCRI recommended quality for key comparisons [21], characterized by a copper half-value layer of 2.482 mm). The measured photon fluence spectrum is shown in Figure 32.

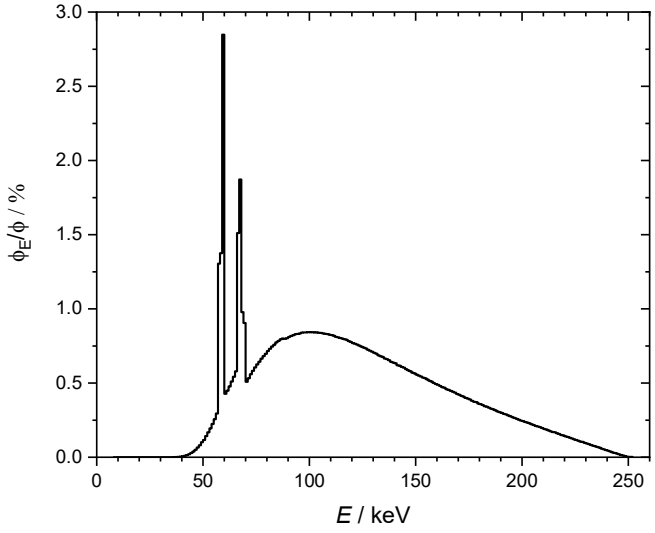

Figure 32. Normalized photon fluence spectrum $\boldsymbol{\phi_E/\phi}$ of the CCRI 250 kV radiation quality.

The largest uncertainty component is caused by the uncertainty of the value of W_{air}/e, without which the remaining uncertainties add up to 0.24%. When two primary free-air chambers are compared to one another, both will use the same value and uncertainty of W_{air}/e, meaning that this large uncertainty component will cancel out.

4.3 Parallel-plate chamber PK400

The parallel-plate free-air ionization chamber type "PK400" (**P**arallelplatten**k**ammer, suitable for measurements up to **400** kV), is used for radiation qualities generated with tube voltages in the 50 kV to 400 kV range. The chamber was conceived, designed and manufactured at PTB and completed as early as 1972. Since then, it has been used as the primary standard for the determination of the quantity exposure/air kerma.

Figure 33. Photo of the free-air chamber type PK400 with (left) and without (right) its lead housing.

4.3.1 Design and dimensions

The design of the PK400 is basically the same as that of the PK100 (Figure 9). It consists of two rectangular, flat, and parallel electrode plates, E_1 and E_2, which are surrounded by the chamber housing. The x-rays enter the chamber through the measuring diaphragm in such a way that the central axis of the blanked x-ray beam runs parallel to the electrodes through the centre of the ion collection volume. The beam exits the PK400 through a hole in the rear wall of the chamber, which is sealed by a thin polyethylene film. The aluminium electrodes, which are about 90 cm high and 86 cm wide, are covered with a 0.5 mm thick graphite layer on the sides facing each other. They are 58 cm apart. Electrode E_1 contains an exchangeable, rectangular, 60 cm high and 5 cm, 10 cm or 20 cm wide collecting electrode E_C separated by a 1 mm wide air gap from the surrounding part of electrode E_1, which serves as the guard electrode E_G. By varying the width of the measuring electrode, the measuring volume of the PK400 can be changed. A voltage of 10 kV is applied between electrodes E_1 and E_2. The guard electrode is at earth potential, while the measuring electrode has a slight potential difference to earth due to the input amplifier of the electrometer. The guard electrode E_G and additional guard strips greatly reduce the distortion of the electric field lines, especially in the vicinity of the electrode edges. The guard strips of the PK400 consist of a total of 32 metal strips (see Figure 33) which are 15 mm wide and bent in a rectangular shape (approx. 90 cm x 86 cm). They are arranged on plexiglass rods parallel to the electrode plates and separated by a 3 mm wide air gap. In this way they span the volume between the electrodes.

Table 12. Main dimensions of the parallel-plate free-air ionization chamber PK400

Item	Dimension
Distance of the polarizing electrodes (E_1 and E_2)	58 cm
Ground electrode (E_G & E_C)	90 cm x 86 cm
High voltage electrode (E_{HV})	90 cm x 86 cm
Height of the collecting electrode	60 cm
Widths of the collecting electrodes	see Table 2
Diameter of the apertures	see Table 2
Outer diameter of the diaphragm	8 cm
Thickness of the diaphragm (made of Densimet® D18)	15 mm
Air path *A* between the reference point in the aperture and the centre	63.15 cm
Thickness of the lead shield at the front of the housing	25 mm
Thickness of the lead shield around the housing (except front wall)	4 mm

The metal strips are electrically connected to each other via the resistors (3 MΩ each) of a voltage divider. A 7.5 cm x 7.5 cm square recess in the metal strip arrangement at the level of the central beam axis at the entry and exit points of the chamber allows the x-rays to pass through unhindered. At these points, the interrupted metal strips are electrically connected with thin graphitized nylon threads. Since the PK400 is used for x-ray beams generated with tube voltages of 50 kV and higher, the attenuation of the radiation by the potential threads is negligible. The housing of the PK400 is lined with 4 mm thick lead, its wall facing the radiation source has 10 mm of lead and is additionally equipped with a 50 cm x 50 cm and 15 mm thick lead plate in the centre around the aperture (left photo in Figure 33). The circular measuring aperture B (see Figure 36) is made of a tungsten-nickel-iron alloy (Densimet® D18) with a density of 18.0 g/cm^3. Its outer diameter is 8.0 cm, its thickness 15 mm. It has an opening which is cylindrical to a depth of 2 mm on the side facing the radiation source. This is followed by a conical part whose opening angle is 1°30' and which was chosen so that this part of the aperture is not directly hit by the radiation of the divergent beam. About 11 cm behind the measuring aperture there is another aperture with a circular opening (diameter 6 cm) between the measuring aperture and the ionization volume that functions to prevents the small amount of secondary radiation produced in the measuring aperture from making any noticeable dose contribution. This additional aperture is not hit by the primary radiation. The apertures can be easily replaced. Apertures with nominal diameters of 10 mm, 15 mm,

20 mm, 30 mm, 40 mm, and 50 mm are used. The design of the measuring apertures prevents them from tilting. The measuring volume of the PK400 is given by the section of the beam whose length *l* in the direction of the beam is given by the width *b* of the measuring electrode and half the width *s* of each of the air gaps of the same size in front of and behind it. The reference point of the PK400 is assumed to be at the point of the measuring aperture on its axis where its cylindrical opening merges into the conical one (see Figure 36). The distance between the reference point in the diaphragm and the centre of the measuring volume is 63.15 cm.

Table 13. Measuring volumes of the parallel-plate free-air ionization chamber PK400

Width of E_c (cm)	5.0257	10.0137	19.9956
Aperture (cm)	Volume (cm^3)		
1.001	3.9551	7.8805	15.7359
1.5001	8.8823	17.6980	35.3399
2.0013	15.8092	31.4999	62.8997
3.0008	35.5435	70.8204	141.4160
4.0003	63.1643	125.8547	251.3098
4.9999	98.6754	196.6107	392.5970

The uncertainty of the aperture diameter is 3 µm and that of the widths is 20 µm. This leads to relative uncertainties of the volume between 0.016% for the largest and 0.072% for the smallest volume.

4.3.2 Chamber model for Monte Carlo simulations

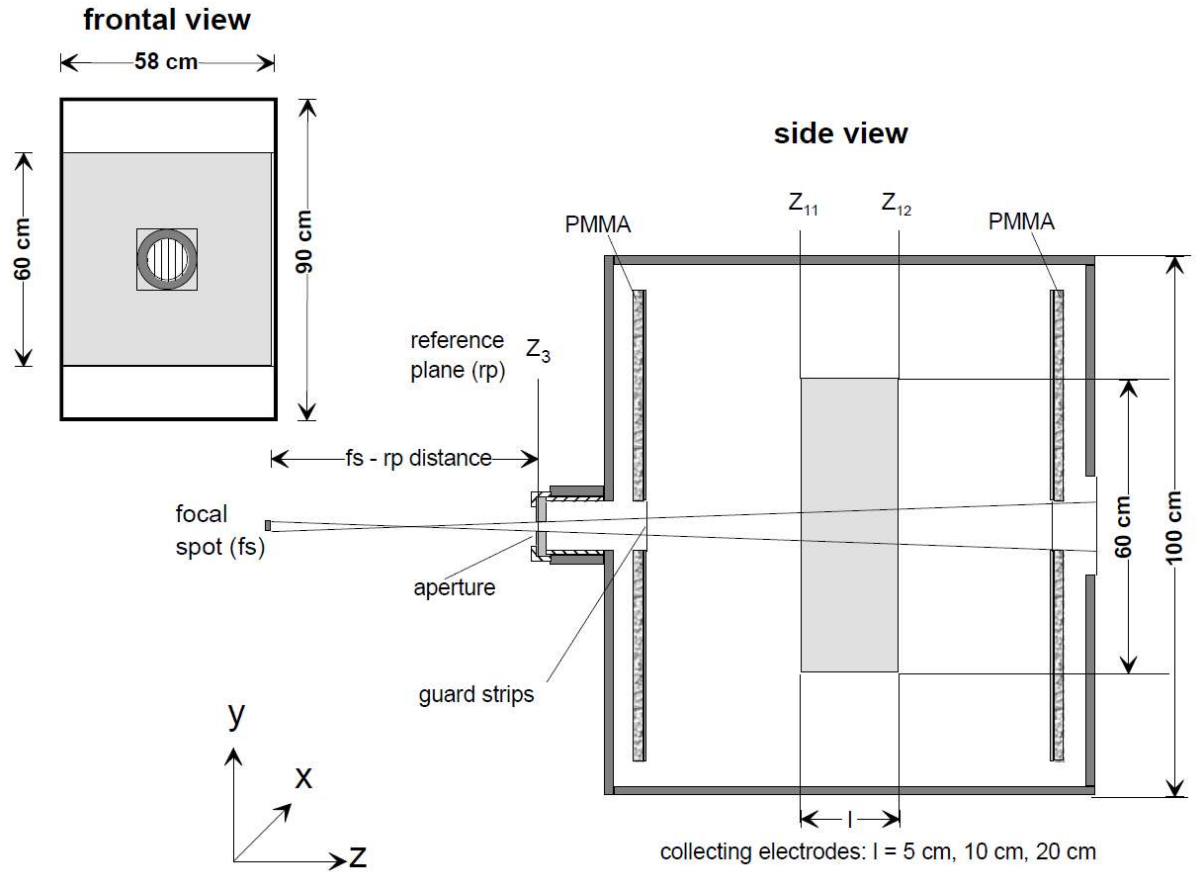

Figure 34. Sketch of the geometry of the PK400 as used in the EGS4-based user code "PK400M".

The transport of x-rays through the PK400 was simulated with the Monte Carlo code system EGS4 [10] as described in section 3.3. The EGS4-based user code designated "PK400M" was developed for this purpose. The geometrical model used for the simulation is shown in
Figure 34. PK400M allows the calculation of the correction factors k_{sc} , k_{e}, k_{dia} and k_{cpe} described in section 3. Details of the calculation methods and results for each correction factor will be given in the following section.

4.3.3 Correction factors for the PK400

Correction for lack of saturation, k_{s}

Saturation effects were measured according to the methods described in 3.2. The correction for initial recombination was found to be k_{si}=1.0007(3). The volume recombination was determined for each of the three different collecting electrodes and was estimated as

$$k_{SV} = 1 + \frac{R_V(E_{c,n})}{U^2} I_{\mathrm{PK400}} \qquad (29)$$

where R_V is a constant in units of V^2/A, given for each single collecting electrode $E_{c,n}$, n = 1, 2, 3 as listed in Table 14, U is the polarizing voltage and I_{PK400} is the chamber current.

Table 14. The constant $\boldsymbol{R_V}$ / U^2 for each of the collecting electrodes of the PK400 at U = 10 kV

Collecting electrode no. and nominal width	R_V / U^2 / A^{-1}
1: 5 cm	$6.85 * 10^6$
2: 10 cm	$3.43 * 10^6$
3: 20 cm	$1.71 * 10^6$

The validity of k_{SV} according to eq. (29) and the data given in Table 14 were confirmed experimentally by the following method. The PK400 was positioned at PTB's x-ray calibration facility at a fixed distance of 100 cm from the x-ray tube. For a selected x-radiation quality (ISO 4037 H-200), the saturation-corrected ionization current of the PK400 was measured at different x-ray tube currents which varied the air kerma rate in the approximate range of 6 mGy/min to 75 mGy/min. This caused the ionization current of the PK400 to vary by a factor of 12 and the k_{SV} to vary from 1.002 to 1.030. The saturation-corrected ionization current of the PK400 was then normalized to the ionization current of the transmission monitor chamber which is always used at the calibration facility and can be assumed to be characterized by a negligible saturation loss in this ionization current range. The suitability of eq. (19) to determine k_{SV} was confirmed by the fact that the normalization factor remains constant within the uncertainty of the measurements (approximately 0.1%) for all tube currents between 1 mA and 30 mA.

Correction for electrical field distortion, k_{d}

The special guard strip design described in 4.3.1 minimizes the distortion of the electrical field at the insides of the front and back edges of the plane parallel capacitor. From the design it can be assumed that there is only a negligibly small distortion at the innermost collecting volume obtained if the shortest collecting electrode with the nominal width of 5 cm is installed at the centre of electrode E_1 (total width of 86 cm) so that k_{d} = 1 applies. To obtain potential influences of distortions for the other collecting volumes with collecting electrodes having nominal widths of 10 cm and 20 cm (and which are hence increasingly closer to the edges of the plane parallel capacitor), the ratio $I(L)$ / L was measured at a fixed

radiation quality and constant tube current, where $I(L)$ is the corrected ionization current measured with the electrode of length L. It turned out that this ratio was almost constant within the estimated relative uncertainty of the measurements (approximately 0.1%). Thus, $k_{\mathrm{d}} = 1.000$ with a relative uncertainty of 0.1% is used for all collecting electrodes.

Correction for air attenuation between reference and measuring point, k_{att}

The air attenuation correction k_{att} along the air path A = 63.15 cm was calculated as a function of monoenergetic photons according to eq. (21). The results are shown in Figure 35. Given the steep increase of k_{att} below about 50 keV it does not make sense to use the PK400 free-air chamber at radiation qualities which are generated with x-ray tube high voltages of less than 50 kV.

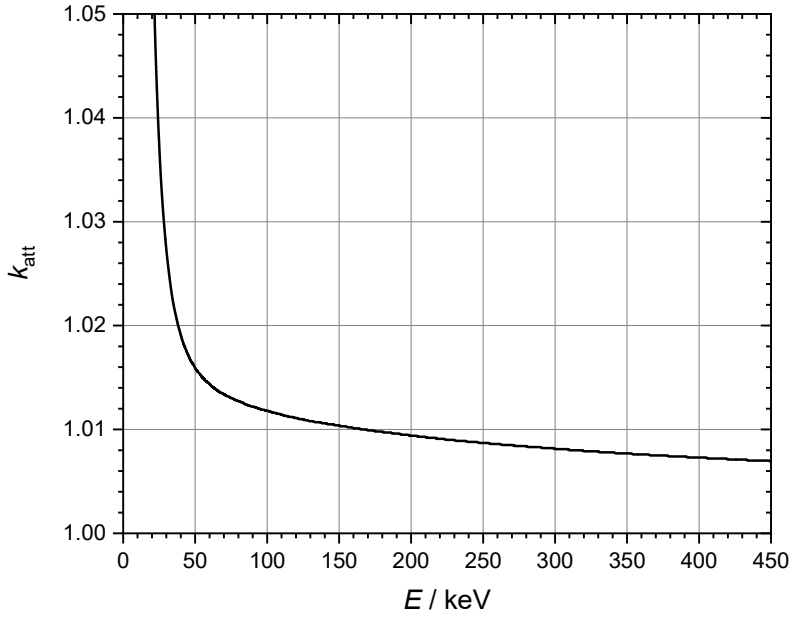

Figure 35. Air attenuation correction k_{att} calculated for the PK400 according to eq. (21) along the air path length A = 63.15 cm.

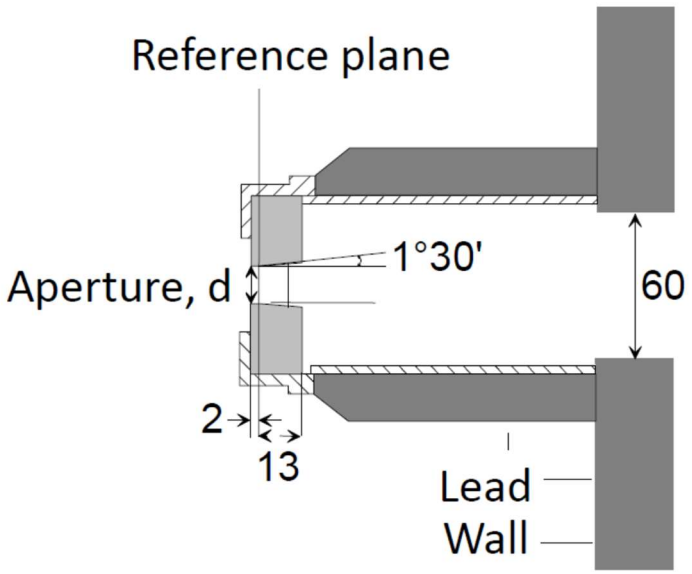

Figure 36. Schematic drawing of the diaphragm as used in the simulation with PK400M. Dimensions are given in mm.

Correction for diaphragm effects, k_{dia}

The model of the diaphragm used in the PK400M Monte Carlo simulation is shown in Figure 36. About 11 cm away from the first aperture there is a second one with a diameter of 60 mm, as shown in Figure 36. This second aperture is larger than the first one, which can have a maximum diameter of 50 mm as described above. Primary photons which pass through the first aperture will also pass through the second one, but scattered photons from the edge of the first aperture will most likely be absorbed by the second aperture edge. The correction k_{dia} is obtained by two simulations with the user code PK400M, one with a nontransparent diaphragm body (by defining a full absorption region around the aperture) and another with the real diaphragm body consisting of Densimet® D18. The correction is calculated as the ratio of the deposited energies in the collecting volume which result from the simulations of the nontransparent and real diaphragms. The results are shown in Figure 37.

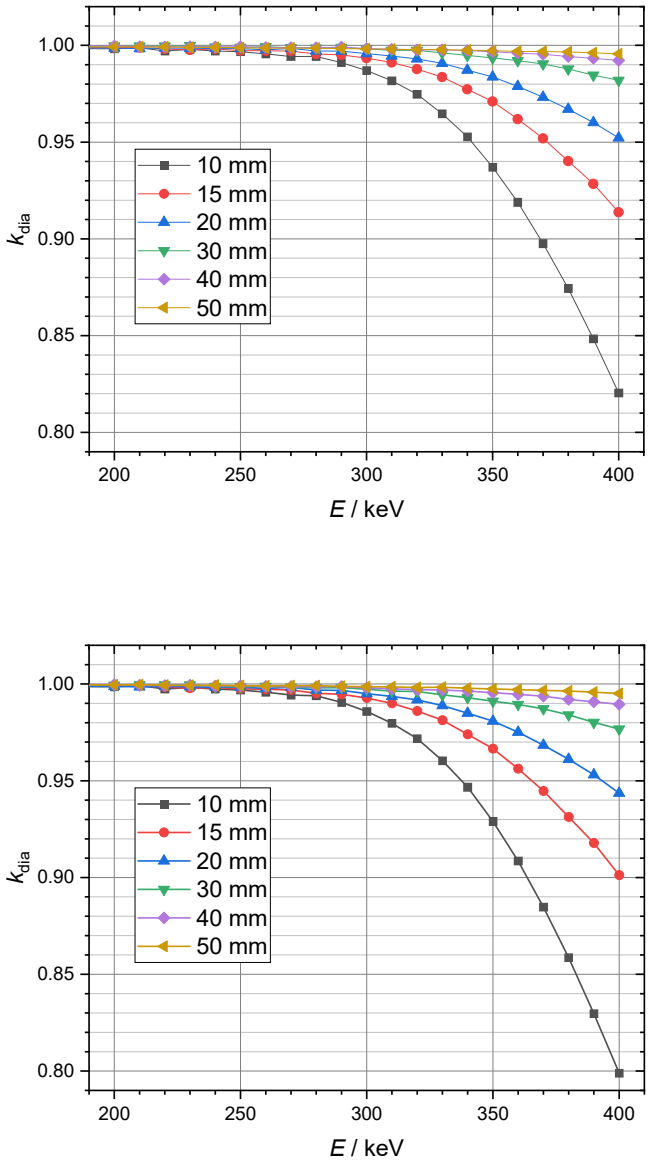

Figure 37. Correction factor k_{dia} calculated as a function of photo energy for aperture diameters 10 mm to 50 mm with a distance of 1 m (upper diagram) and 3 m (lower diagram) between the reference plane and the x-ray focus.

The correction k_{dia} becomes significant above 250 keV and is largest at 400 keV. It decreases with increasing aperture diameters because the fraction of photons transmitted through the diaphragm body to those passing through the aperture decreases. Corrections at 3 m distance are slightly larger than the corresponding values at 1 m because the divergence of the beam decreases with increasing distance from the source and thus the path lengths of the photons through the diaphragm body are shorter.

Correction for scattered photons in the air of the PK400, k_{sc}

The correction k_{sc} was calculated by means of the PK400M simulation program. Two simulations were made, one with and one without the transport of air scattered photons. In the latter simulation, only the secondary electrons after the first interaction of the primary photons were transported, but not the scattered photons (fluorescence and Compton photons). Diaphragm effects were excluded by choosing a beam diameter equal to the aperture diameter. k_{sc} was obtained as the ratio of the deposited dose in the collecting region calculated without and with scattered photons. This ratio is less than one because the contribution from scattered photons increases the deposited dose. Figure 38 shows the results obtained in this way for k_{sc} as a function of monoenergetic photons in the range from 10 keV to 450 keV. The interpretation of the curve corresponds to that of the other two FACs presented in this report (Figure 16 and Figure 29).

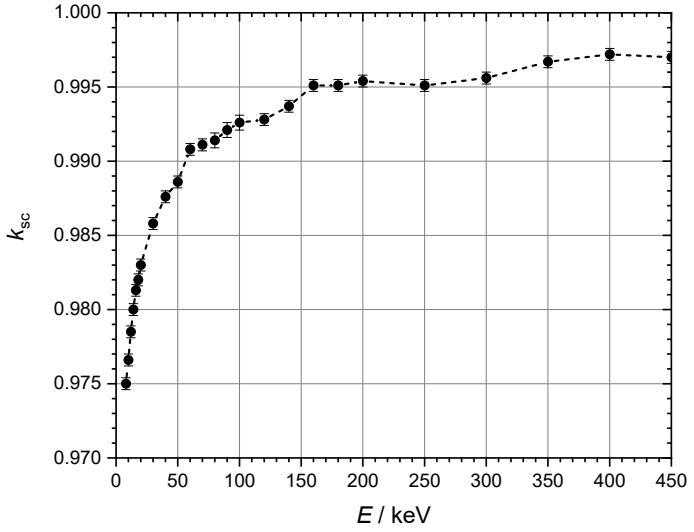

Figure 38. Correction factor k_{sc} calculated as a function of the photon energy.

Correction for electron loss, k_{e}

A simulation with PK400M was made that excluded diaphragm effects and air attenuation. Only one photon interaction was allowed and only the secondary electrons were transported. The correction k_{e} was calculated as the ratio of the true value of the air kerma and the deposited dose in the collecting volume under these conditions. The relative statistical uncertainty was less than 0.02%. The results obtained for photon energies up to 430 keV are shown in Figure 39 for aperture diameters 10 mm and 30 mm. Up to a primary photon energy of 160 keV, the range of the photoelectrons (CSDA range in air about 30 cm) is not sufficient to cause a significant loss of energy deposition within the ion collection volume. Because of the small contribution of the energy transferred to photoelectrons compared to the total energy transferred to electrons (1.1% and 0.2% at 200 keV and 300 keV, respectively), the ionization loss remains below 0.2% up to 320 keV. Above 320 keV, the first Compton electrons have sufficient kinetic energy to leave the collection volume. At higher photon energies, the energy deposition loss in the collection volume increases strongly due to the increasingly energetic Compton electrons. A

significant difference between the calculations for the 1.0 cm and 5.0 cm diameter apertures becomes apparent within the statistical uncertainty of 0.02% at energies greater than 400 keV.

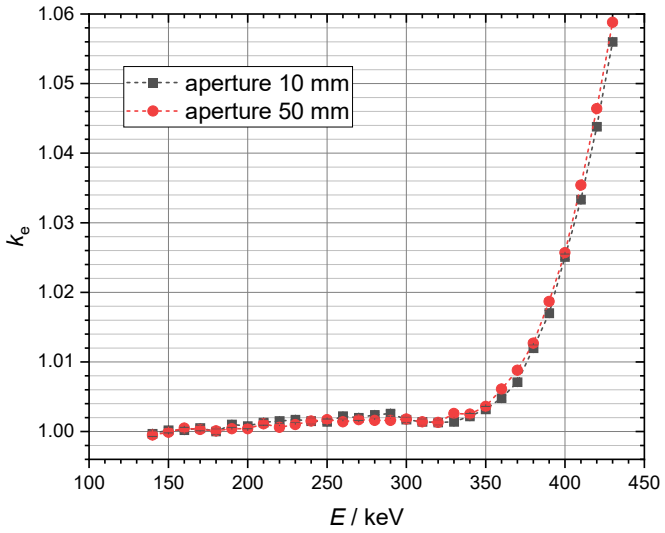

Figure 39. Correction factor k_e as a function of the photon energy calculated for apertures of diameter 10 mm and 50 mm.

Product of correction factors, k

The product of correction factors k is defined as

$$k = k_{att}\, k_d k_{dia} k_{sc} k_e k_{iw} \tag{30}$$

Figure 40 shows the product of the correction factors as a function of the energy of the primary photons. The curves shown in the upper diagram were calculated for the measuring volume with a measuring electrode length of l = 20 cm and apply to a focus-reference distance of 100 cm and to the aperture diameters of 1.0 cm to 5.0 cm. Below 50 keV, the curves rise steeply due to the significant increase in air attenuation here. From 50 keV to about 300 keV, the curves remain at a nearly constant level close to 1.005 before branching out at higher energies to higher or lower values depending on the aperture diameter. This behaviour can be explained by the strong increase of the correction factor for the path length limitation of the secondary electrons above 350 keV (Figure 39) with a simultaneous strong decrease of the correction factor for the aperture edge transmission (Figure 37), which weakens as the diameter of the aperture becomes larger. At an aperture diameter of 1.0 cm, the correction factor k_{dia} dominates, causing the curve to fall, while at an aperture diameter of 5.0 cm, the correction factor k_e dominates, causing the curve to rise. At the aperture diameter of 3.0 cm these two opposing contributions almost offset one another. The lower diagram of Figure 40 shows separately the part of the curve for the 3.0 cm aperture diameter within a scale of 1.00 and 1.03. The energy range for which the PK400 can reliably be used as a primary standard for air kerma measurements can be read from the diagram shown in the figure. For energies below 50 keV, the correction factors for air attenuation increase steeply. Therefore, larger uncertainties must be expected when using the chamber for generating voltages below 50 kV. k varies by no more than about 0.4% between 50 keV and 350 keV, which qualifies this chamber for air kerma measurements in this energy region. For apertures greater than 15 mm, the PK400 can be used for x-ray qualities with generating voltages up to 400 kV.

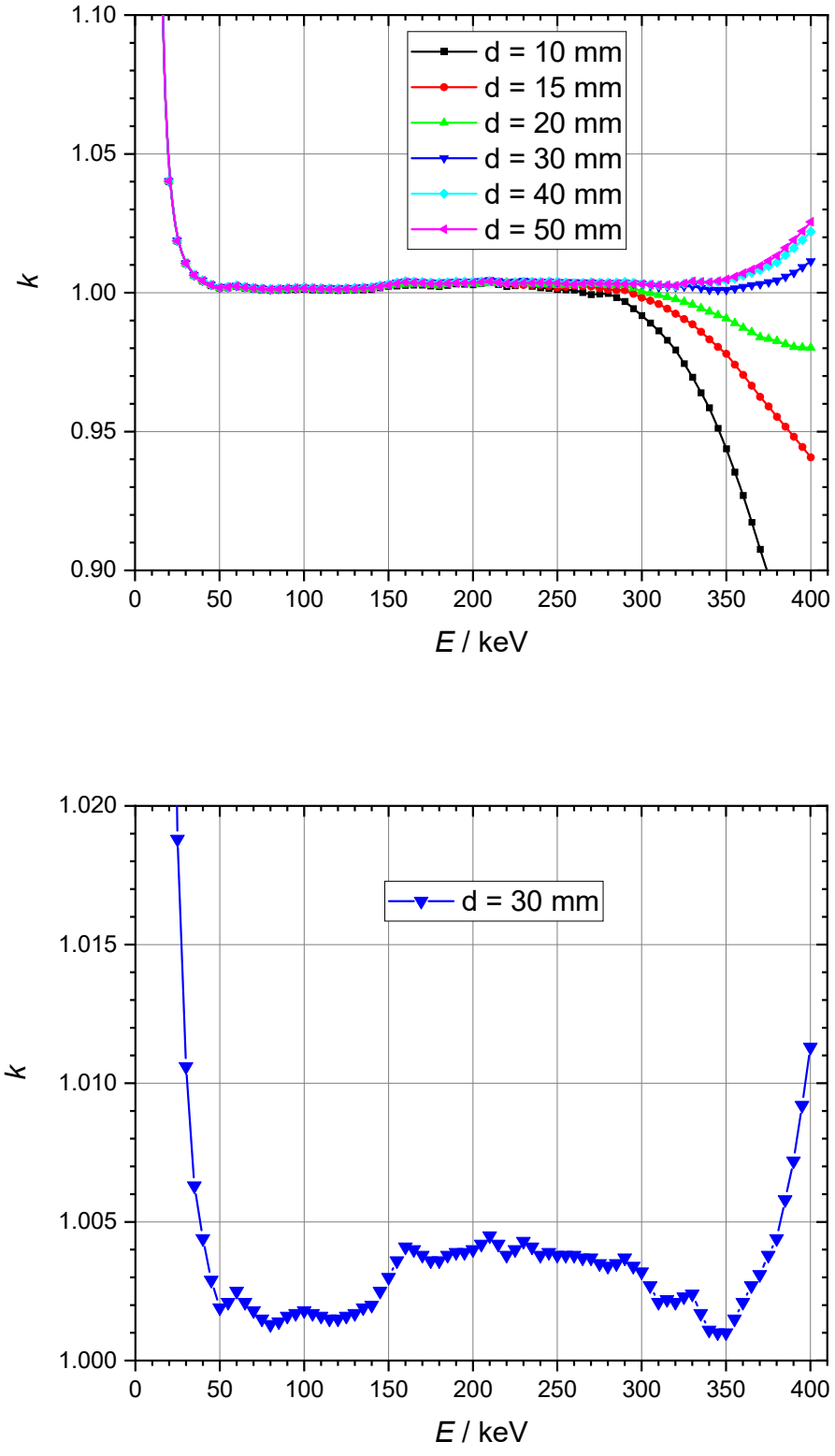

Figure 40. Product of all correction factors *k* calculated for the 5 cm collector electrode of the PK400 and all available apertures (upper diagram) and of the aperture of diameter 30 mm with enlarged scale (lower diagram) at a focal spot to reference plane distance of 100 cm.

4.3.4 Uncertainty of the air kerma rate determined with the PK400

The air kerma rate measured with the PK400 is obtained from the following equation:

$$\dot{K}_{\text{air}} = \frac{W_{\text{air}}}{e} \frac{I}{\varrho_{\text{air}} V} \frac{1}{1-\bar{g}} k_h k_{iw} k_{pol} k_s k_d k_p k_\rho k_{att}\ k_{sh} k_{dia} k_{sc} k_e \qquad (31)$$

In practice, air kerma rates are measured for defined reference x-radiation qualities. The PK400 is well suited for radiation qualities generated with tube voltages in the 50 kV to 400 kV range. The correction factors for x-radiation qualities characterized by their photon fluence spectra ϕ_E with maximum energies E_{max} are obtained as the air-kerma-weighted mean values $\bar{k}$ according to eq. (25).

Table 15. Uncertainty budget estimated for the radiation quality ISO 4037 N400, collecting electrode of width 20 cm and aperture of diameter 3 cm.

Parameter	Description	Value	u_{iA} (%)	u_{iB} (%)	u_{i} (%)
W_{air}/e	Mean energy (eV)	33.97		0.35	0.35
I	Ionization current	-	0.10	0.06	0.12
ρ_{air}	Air density (kg m^{-3})	1.2048		0.01	0.01
V	Collecting volume (cm^3)	141.416	0.05		0.05
$1/(1-\bar{g})$	Radiative loss correction	1.0003		0.02	0.02
k_h	Humidity	0.9980		0.04	0.04
k_{iw}	$= k_{\text{ii}} k_{\text{W}}$ (section 3.2)	0.9995		0.11	0.11
k_{pol}	Polarity	1.0000	0.05		0.05
k_s [1)]	Saturation	1.0029	0.05		0.05
k_d	Field distortion	1.0000		0.10	0.10
k_p	Wall penetration	1.0000	0.05		0.05
k_ρ	Air density correction	1.0000	0.036		0.036
k_{att}	Air attenuation	1.0081		0.05	0.05
k_{dia}	Diaphragm effects	0.9983		0.05	0.05
k_{sc}	Scattered radiation	0.9956		0.05	0.05
k_e	Electron loss	1.0018		0.05	0.05
$\dot{K}_{\text{air}}$	Air kerma rate (result)	-	0.19	0.39	0.43

[1)] Calculated for the air kerma rate 0.25 mGy/s

The uncertainty budget shown in Table 15 was estimated for an ISO4037 N400 quality [24] generated with a W-anode tube at 400 kV and added filtration of 4 mm Al, 6 mm Sn and 10 mm Pb, characterized by a copper half-value layer of 7.25 mm. The measured photon fluence spectrum is shown in Figure 41.

The largest uncertainty component is caused by the uncertainty of the value of W_{air}/e, without which the remaining uncertainties add up to 0.24%. When two primary free-air chambers are compared to one another, both will use the same value and uncertainty of W_{air}/e, meaning that this large uncertainty component will cancel out.

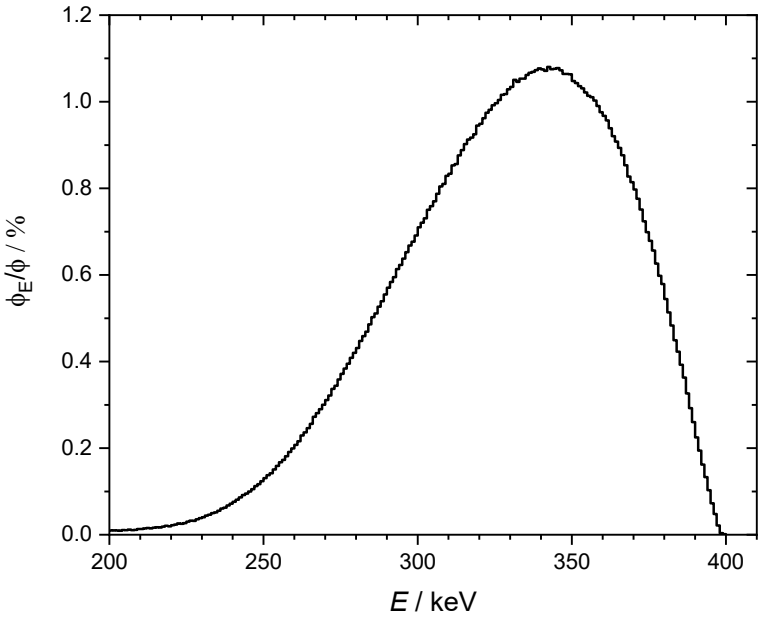

Figure 41. Normalized photon fluence spectrum $\boldsymbol{\phi_E/\phi}$ of the ISO4037 N400 [24] radiation quality.

5 Summary

This technical report describes in detail the three types of free-air ionization chambers currently used at the Physikalisch-Technische Bundesanstalt (PTB) in Germany for the primary measurement of the quantity air kerma. These ionization chambers cover measurements at x-ray qualities generated with tube high voltages in the 7.5 kV to 400 kV range. All factors required for calculating the air kerma from the measured ionization charge are explained in this report and their values are listed in tables or shown in diagrams. The relative standard uncertainty of the air kerma measurements are estimated for selected x-ray qualities and result in a value of about 0.45% for all chamber types. The largest component uncertainty, 0.35%, is caused by the uncertainty of the value of W_{air}/e, which is the mean energy needed to produce an ion pair in dry air. The expanded relative uncertainty for a coverage factor $k = 2$ of secondary air kerma standards calibrated at PTB against their primary standards is usually of the order of 1%.

References

[1] ICRU, “REPORT No. 85: FUNDAMENTAL QUANTITIES AND UNITS FOR IONIZING RADIATION (Revised),” *J. ICRU*, vol. 11, no. 1, pp. 33–33, 2011.

[2] D. T. Burns and L. Büermann, “Free-air ionization chambers,” *Metrologia*, vol. 46, no. 2, 2009.

[3] J. W. BOAG, “Ionization Chambers,” in *The Dosimetry of Ionizing Radiation*, Academic Press, 1987, pp. 169–243.

[4] M. T. Niatel, “Etude expérimentale de l’influence de la vapeur d’eau sur l’ionisation produite dans l’air,” *C.R. Acad. Sci. Paris*, vol. B. 268, p. 1650, 1969.

[5] M. T. Niatel, “Influence de la vapeur d’eau sur l’ionisation l’air dans le cas d’une chamber a cavité,” *C.R. Acad. Sci. Paris*, vol. B. 281, p. 361, 1975.

[6] ICRU, “ICRU Report 31: Average Energy Required to Produce an Ion Pair,” *J. ICRU*, vol. 31, 1979.

[7] L. Büermann *et al.*, “Measurement of the x-ray mass energy-absorption coefficient of air using 3 keV to 10 keV synchrotron radiation,” *Phys. Med. Biol.*, vol. 51, no. 20, pp. 5125–50, Oct. 2006.
[8] H. Buhr, L. Büermann, M. Gerlach, M. Krumrey, and H. Rabus, “Measurement of the mass energy-absorption coefficient of air for x-rays in the range from 3 to 60 keV,” *Phys. Med. Biol.*, vol. 57, no. 24, pp. 8231–8247, 2012.
[9] H. G. Menzel, “Key Data for Ionizing-Radiation Dosimetry: Measurement Standards and Applications,” *J. ICRU*, vol. 14, no. 1, pp. 1–118, 2014.
[10] W. R. Nelson, H. Hirayama, and D. W. O. Rogers, “The EGS4 code system,” *Stanford Linear Accel. Cent. Rep.*, no. SLAC-265, 1985.
[11] A. F. Bielajew and D. W. O. Rogers, “PRESTA: The parameter reduced electron-step transport algorithm for electron Monte Carlo transport,” *Nucl. Instr. Meth. B*, vol. 18, pp. 165–181, 1987.
[12] D. W. O. Rogers, “How accurately can EGS4/PRESTA calculate ion-chamber response?,” *Med. Phys.*, vol. 20, no. 2, pp. 319–323, Mar. 1993.
[13] A. F. Bielajew and I. Kawrakow, “PRESTA-I -> PRESTA-II: The new physics,” *KEK Proc.*, vol. 97–16, 1997.
[14] Y. Sakamoto, “PHOTX data as PEGS4 photon cross section data,” *KEK Proc. 93-15*, 1993.
[15] H. Hirayama, N. Yoshihito, and B. Shuichi, “Implementation of an L-shell Photoelectron and an L X-ray for Elements into the EGS4 Code,” *KEK Intern. 95-10*, 1995.
[16] A. Del Guerra, W. R. Nelson, and P. Russo, “A simple method to introduce K-edge sampling for compounds in the code EGS4 for x-ray element analysis,” *Nucl. Instr. Meth. A*, vol. 306, pp. 378–385, 1991.
[17] Y. Namito, S. Ban, and H. Hirayama,“LSCAT: Low-energy photon-scattering expansion for the EGS4 code,” *KEK Intern. 95-10*, 1995.
[18] S. M. Seltzer, “Calculation of photon mass energy-transfer and mass energy-absorption coefficients,” *Radiat. Res.*, vol. 136, no. 2, pp. 147–170, 1993.
[19] S. Ketelhut, L. Büermann, and G. Hilgers, “Catalog of x-ray spectra of Mo-, Rh-, and W-anode-based x-ray tubes from 10 to 50 kV,” *Phys. Med. Biol.*, vol. 66, no. 11, 2021.
[20] T. W. Grimbergen, E. van Dijk, and W. de Vries, “Correction factors for the NMi free-air ionization chamber for medium-energy x-rays calculated with the Monte Carlo method,” *Phys. Med. Biol.*, vol. 43, no. 11, pp. 3207–24, Nov. 1998.
[21] CCEMRI Section I, “Qualités de rayonnement,” *2me réunion R15-R16*, 1972.
[22] D. T. Burns, C. Kessler, and L. Büermann, “Key comparison BIPM.RI(I)-K2 of the air-kerma standards of the PTB, Germany and the BIPM in low-energy x-rays,” *Metrologia*, vol. 51, no. 06011, 2014.
[23] D. T. Burns, C. Kessler, and L. Büermann, “Key comparison BIPM.RI(I)-K3 of the air-kerma standards of the PTB, Germany and the BIPM in medium-energy x-rays,” *Metrologia*, vol. 51, no. 06016, 2014.
[24] International Standardization Organization, “Radiological protection — X and gamma reference radiation for calibrating dosemeters and doserate meters and for determining their response as a function of photon energy — Part 1: Radiation characteristics and production methods,” *ISO 4037-1*, 2019.